Chapter 7

Blended and Multicomponent Cements Based on Strontium Aluminate

1. Blended cements

The term **blended cement** (**multicomponent cement**) is usually used to denote inorganic binder that contains a mineral additions in combination with Portland cement and often also with calcium sulfate. Blended cements usually contain single blending component as an addition, in the case that two or more blending component are applied, the term **multicomponent cement** is used. A variety of industrial by-products and natural materials quantify as mineral additions, and may be used as constituents of inorganic binders of cementitious systems. These materials may possess their own cementitious properties, or they may be latent hydraulic, pozzolanic, or even non-reactive [12,387,599-601].

1. **Hydraulically reactive materials**: these materials exhibit the cementing properties when mixed with water, without the presence of any other constituent acting as activator. Some fluidized-bed ashes or industrial slags are the examples of such materials [602-604].

2. **Latent hydraulic materials**: are also able to react hydraulically, but only in the presence of at least small amounts of suitable activator ($Ca(OH)_2$, NaOH or $CaSO_4$). They are usually glassy or amorphous and contain significant amount of CaO, SiO_2 and Al_2O_3. Blast furnace slag (Fig.1(c)) is the most widely used latent hydraulic material [505,506].

3. **Pozzolanic materials or pozzolans**: when mixed only with water, they do not exhibit cementing properties. These materials can react with calcium hydroxide in the presence of water at ambient temperatures, to form calcium silicate/aluminate hydrates. Variety of materials of natural or artificial origin, such as fly ash, microsilica (Fig.1(a)), calcined clays (b) and shales, diatomaceous earth, etc.have these properties [3,607-610].

4. **Non-reactive constituents of inorganic cements**: do not react chemically, but modify the rheology of fresh paste and some properties of hardened material.

ASTM C2 19 defines blended hydraulic cement as hydraulic cement consisting of two or more inorganic constituents (at least one of which is not Portland cement or Portland cement clinker) which separately or in combination contribute to the strength gaining properties of cement (made with or without other blendings constituents, processing additions and functional additionsadded during grinding) and are added by intergrinding or blending.

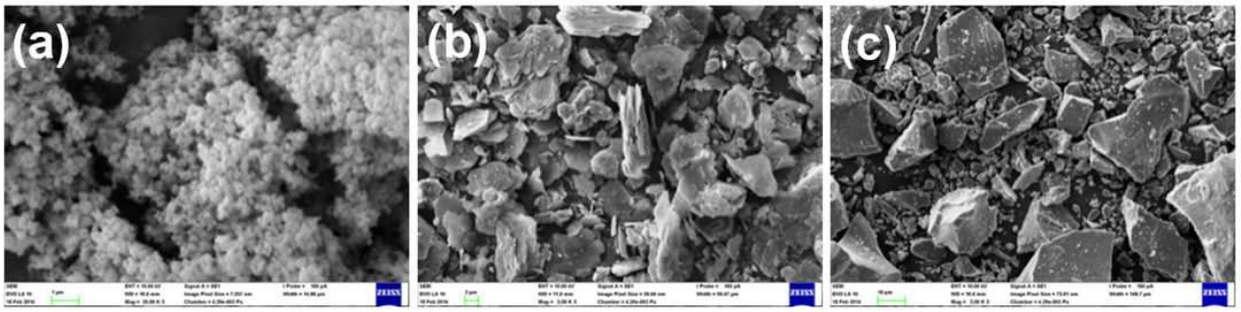

Figure 1. SEM image of microsilica (a), calcined kaolin (b) and blast furnace slag (c).

The types of blended cements covered by this specification are divided as follows [611]:

Portland blast-furnace slag cement;

Portland-pozzolan cement;

Slag cement;

Pozzolan-modified Portland cement;

Slag modified Portland cement.

1.1. Blends of strontium aluminate and aluminate cement

The effect of calcium aluminate onto the hydration of strontium aluminate was investigated by the calorimetric experiment (Fig.2) using the blend of both constituents. Isothermal calorimetric measurement shows that the main hydration effect of calcium aluminate cement[1] is delayed in time, the peak height decreases while the peak width increases with increasing content of strontium aluminate in the mixture. The effect of fast evolution of heat after mixing strontium aluminate cement with water (Chapter 5.2) increases with the content of it the sample. After the first 95 hours of hydration the hydration curves of all samples drop down to the baseline, but the cements still produces the heat flow of 0.09 (Secar 51), 0.11 (20:1), 0.09 (10:1), 0,20 (5:1), 0.08 $J \cdot g^{-1}$ (1:1).

Therefore, increasing amount of SrAC in CAC increases instantaneous heat released immediately after mixing with water and also increases the length of induction period and the width of the main hydration effect.

Hexagonal CAH_{10} hydrate as the main product of hydration was recognized by powder XRD analysis of the product of hydration (Fig.3). Furthermore, the diffraction lines of the rest of unhydrated calcium aluminate ($CaAl_2O_4$) and minor constituents of applied AC such as tetragonal gehlenite ($Ca_2Al_2SiO_7$) and calcium titanium iron oxide ($Ca_3TiFe_2O_8$), appeared.

The scanning electron microscopy of hydrated cement stone (Fig.4) shows the formation of well crystallized hexagonal product of CAH_{10} (Table 6.1). The hydrates of acicular crystal

1 Information about the hydration of AC cement can be found in Chapter 5 and 6.

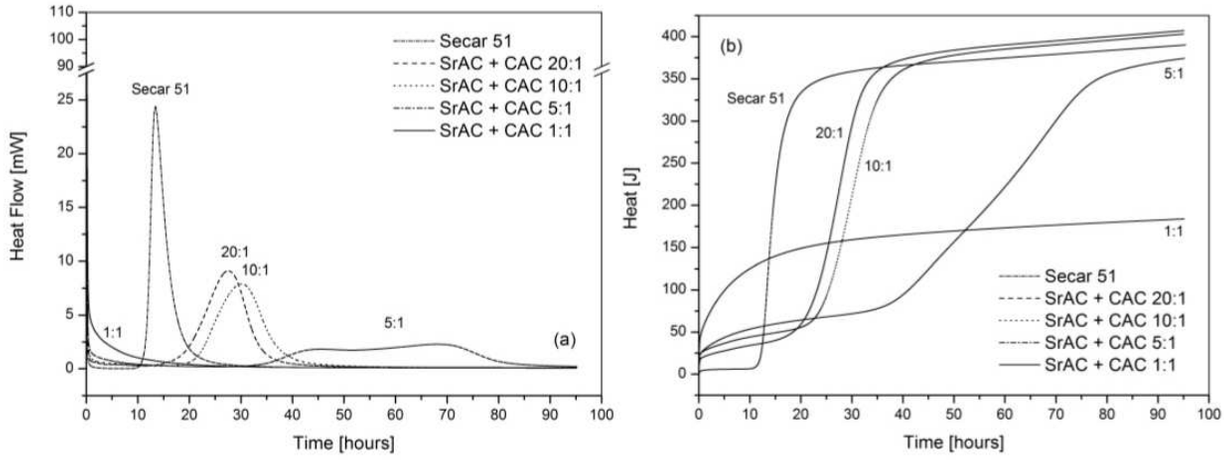

Figure 2. Heat flow (a) and heat of hydration (b) for the blend of strontium aluminate and calcium aluminate cement.

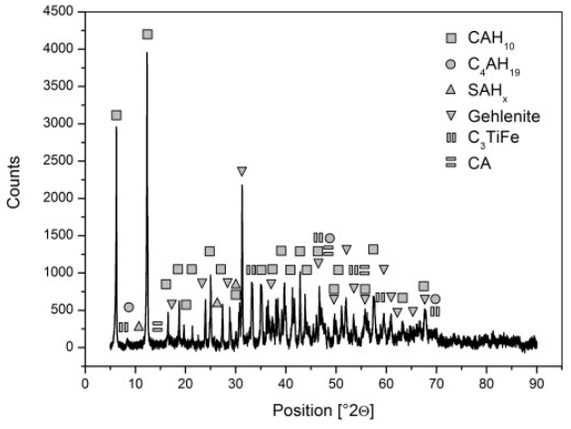

Figure 3. X-ray diffraction analysis of cement stone of SrAC and CAC blend in the mass ratio of 10:1.

character composed of radiating mass of slender, needle-like crystals with the hexagonal base were formed. These crystals are the main product of hydration in multicomponent AC cement as well (Chapter 7.4).

Thermal analysis of hydrated sample (Fig.5(a)) shows huge endothermic peak at 120 °C and smaller endothermic peat at 250 °C. The first effect is caused by the loss of molecular water of CAH_{10}. Since much water is bound very weakly, the water loss starts with drying. The peak intensity and its shape are then affected by initial drying of the specimen as well. The dehydration of crystalline CAH_{10} takes place in two steps. Firstly, interlaminar water is released and subsequent loss of water leads to the collapse of the structure. In the case that water cannot evaporate easily, the thermal decomposition of monocalcium aluminate hydrate leads to the tricalcium aluminate hexahydrate (C_3AH_6, hydrogarnet) and cubic phase of gibbsite (AH_3):

$$3\,CAH_{10} \rightarrow C_3AH_6 + 2\,AH_3 + 18\,H \quad (1)$$

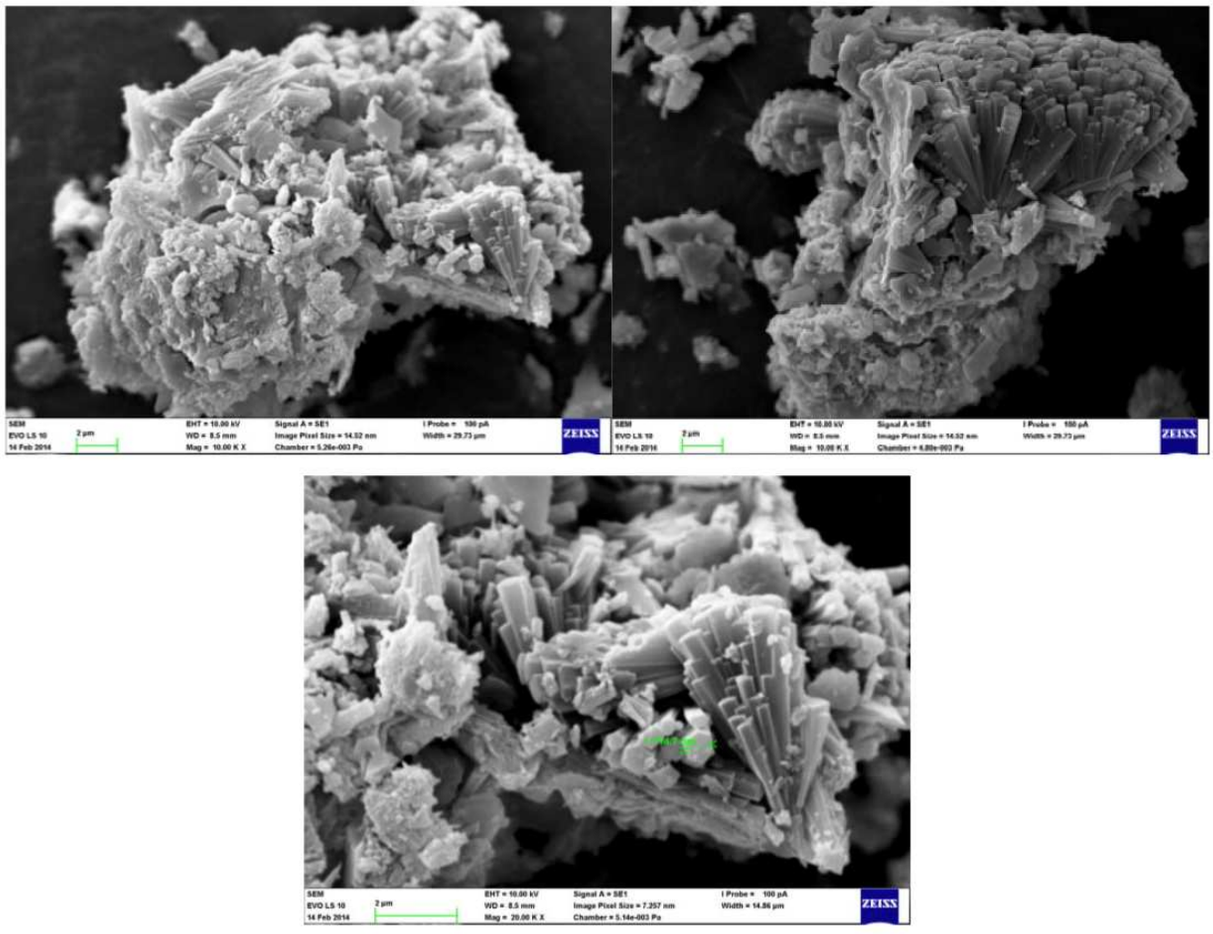

Figure 4. SEM image of hydrated cement stone of AC and SrA blend in the mass ratio of 10:1.

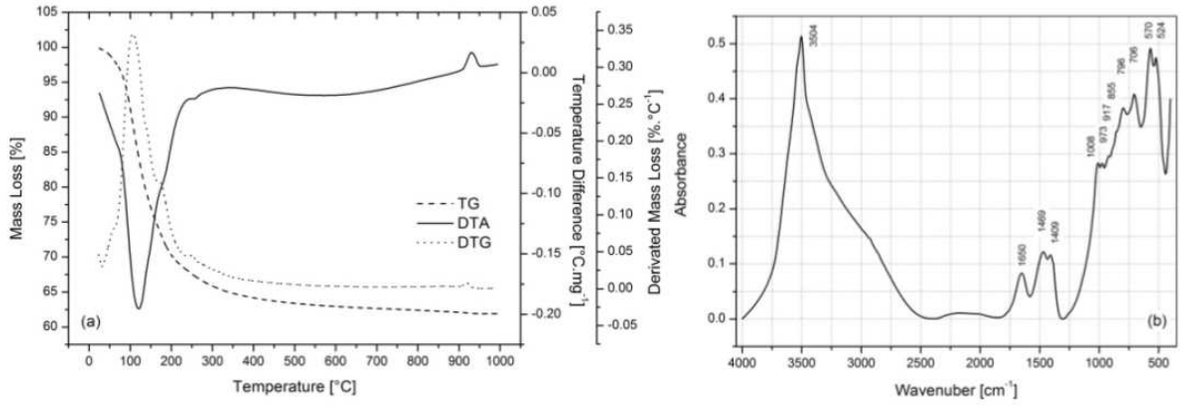

Figure 5. Thermal analysis (a) and infrared spectroscopy (b) of hydrated cement stone.

The second small peak is attributed to the dehydration of AH_3, C_3AH_6 [7,12,269,612] and Sr_3AH_6 (please see Chapter 6.5). The dehydration of hydrogarnet leads to the mayenite (dodeca-calcium heptaaluminate, $C_{12}A_7$) and $Ca(OH)_2$ [613]:

$$7\,C_3AH_6 \rightarrow C_{12}A_7 + 9\,CH + 33\,H \quad (2)$$

The thermal decomposition of calcium hydroxide takes place within the temperature range from 350 to 450 °C [613]. As the consequence of gradual dehydration of $C_{12}A_7$ (mayenite contains 1.3 % of water which corresponds to the formula $C_{12}A_7H$ [12,613]), the mass of sample decreases to the temperature of 900 °C. The effect on the right shoulder of DTA and DTG peak that appears near to the temperature of 170 °C indicates the presence of C_2AH_8 in the hydrated sample [483].

Infrared spectrum of hydrated cement stone is shown in Fig.5(b). In general the strong and broad band observed around 3400–3000 cm^{-1} corresponds to the OH stretching vibration of adsorbed water and water in formed hydrates. The maximum located at 3505 cm^{-1} belongs to the hydroxyl stretching vibration of hexagonal CAH_{10}. Water bending mode is placed at the wavenumber of about 1650 cm^{-1}. The band $\nu_3(CO_3^{2-})$ around 1410 cm^{-1} indicates the presence of both, calcium and strontium carbonate. The $\nu_2(CO_3^{2-})$ is very weak, but still recognizable part of the complex region below 1200 cm^{-1}. These features are located at 878 ($CaCO_3$) and 855 cm^{-1} ($SrCO_3$). The band at 1008 cm^{-1} was assigned to the stretching of Al-O bond.

The low-frequency rotational modes of hydroxyl groups (=Al-OH) of C_2AH_8 (920 and 705 cm^{-1}) and CAH_{10} (970 and 795 cm^{-1}) confirm the presence the both hydrates in the sample which were implied from the results of thermal analysis. The doublet band, that reaches the maximum at the wavenumber of 570 and 525 cm^{-1} is placed in the spectral region of characteristic frequency of the Al-O-Al stretching of AlO_6 octahedra [483,614].

1.2. Blends of strontium aluminate and Portland cement

Calorimetric data for the hydration of blend of strontium aluminate and Portland cement is shown in Fig.6.

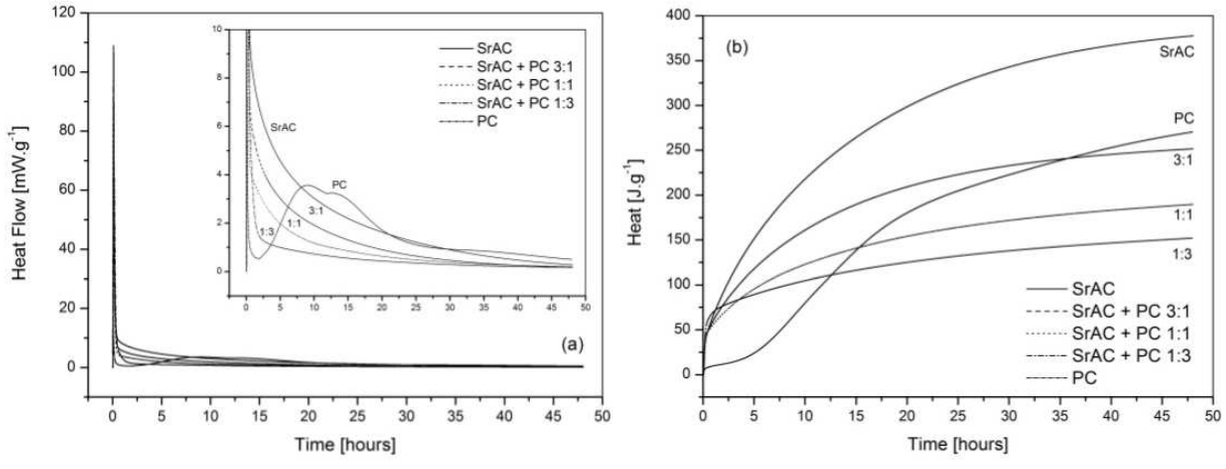

Figure 6. Heat flow (a) and heat of hydration (b) for the first 50 h of hydration of the mixture of strontium aluminate cement with Portland cement.

The heat on hydration decreases with increasing content of Portland cement in the blend. The heat flow released after mixing with water decreases more rapidly for the mixtures with higher content of Portland cement. Moreover, the comparison of calorimetric data measured for pure PC with the results of blended cement shows, that there areno measured features related to the original Portland cement.

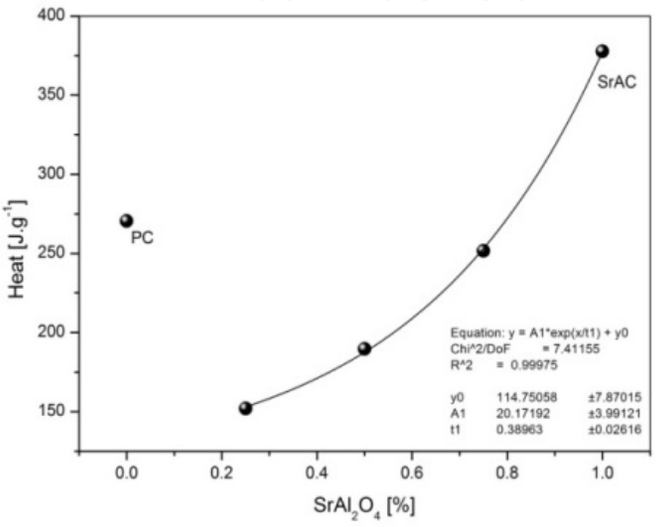

Figure 7. Influence of PC on hydration heat released by SrAC during the first 48 h of hydration.

The hydration heat released during the first 48 hours of hydration shows the highest value for strontium aluminate clinker which decreases with decreasing content of strontium aluminate clinker according to the exponential law (Fig.7). After the first 48 hour of hydration allcurves already drop down to the baseline, but the cements still produce heat flows of 0.28 (SrAC), 0.28 (3:1), 0.20 (1:1), 0.18 (1:3) and 0.50 $mW \cdot g^{-1}$ (PC). Thus the value of heat flow decreases with the content of Portland cement in the blend.

Observed decrease of heat released during the hydration of blends with increasing content of the Portland cement should be explained by the layer of hydration product of PC and ettringite formed on the surface of SrAC grains. Higher content of Portland cement also means increasing amount of gypsum in the sample and hence higher amount of ettringite, which can be formed. That often pronounces the possibility to use strontium aluminate cement as the expansion or shrinkage compensation additive as is discussed in Chapter 8.

After the calorimetric experiment, the hydration was stopped by the same way as was described in Chapter 8.3 in order to carry out the XRD, TG-DTA and IR analyses of hydrated cement stone.The SEM analysis of cement stone after the first 48 h of hydration shows the effect of Portland cement on the morphology of hydrated cement stone. The most significant features are higher amount of formed ettringite in the blends with higher content of Portland cement, i.e. higher amount of gypsum (Fig.10 and Fig.11), while only rare AFt crystals can be found in SEM images of the sample with only 25 % of Portland cement (Fig.8).

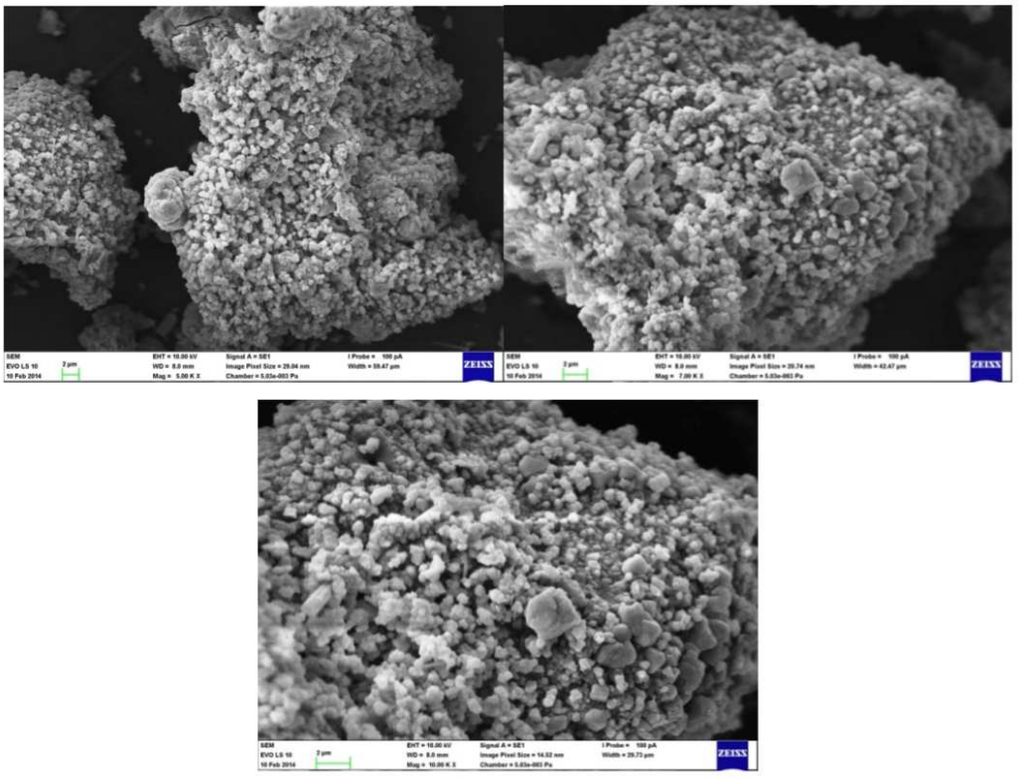

Figure 8. The hydrated cement stone prepared from the mixture of SrAC and PC (3:1).

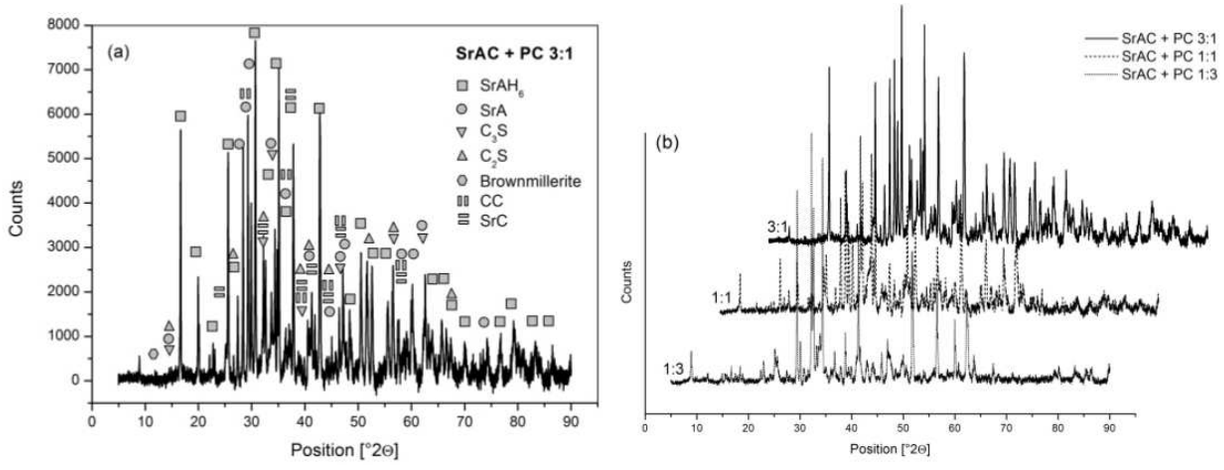

Figure 9. X-ray diffraction analysis of the blend of strontium aluminate cement with Portland cement.

Large amount of formed ettringite in the blend with the highest content of Portland cement was also recognized in XRD pattern of hydrated cement stone (Fig.9). It is an interesting fact, that the features of ettringite not only disappear from the diffraction pattern, but are substituted by growing diffraction lines (18.35, 17.43, 15.43, 25.04 and 22.34° on 2Θ scale) of

new phase. It could be supposed, that is formed with increasing content of strontium aluminate cement in the blend.

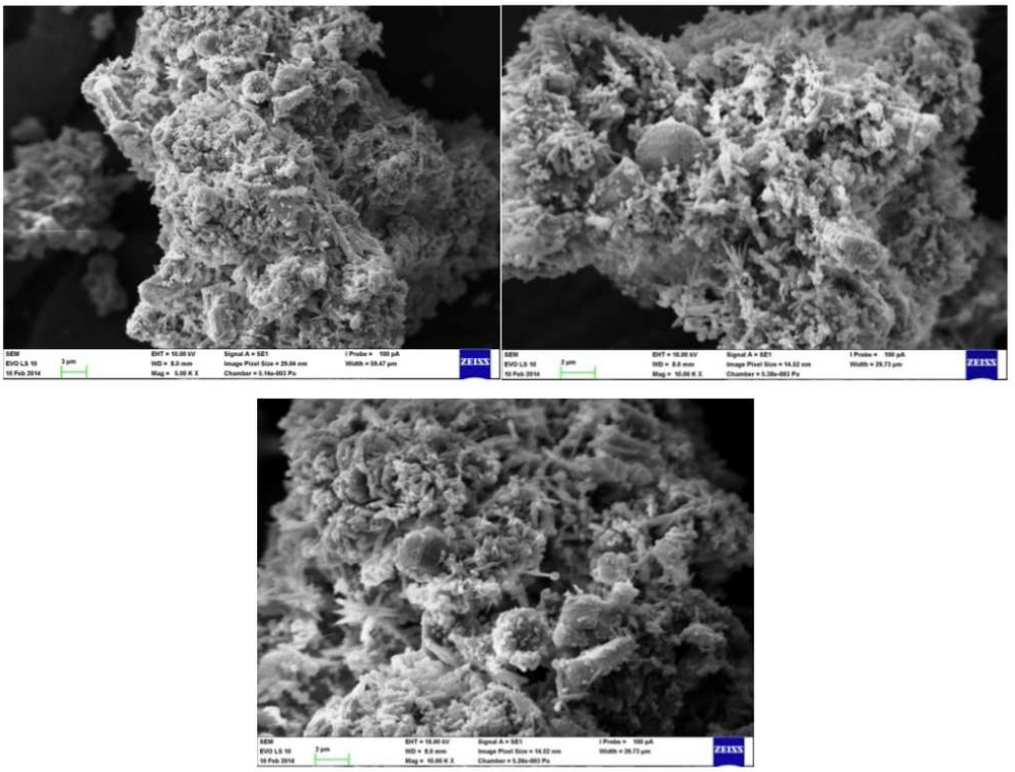

Figure 10. The hydrated cement stone prepared from the mixture of SrAC and PC (1:1).

Infrared spectrum of hydrated cement stone shows that the intensity of band related to the stretching of OH groups of tri-strontium aluminate hexahydrate decreases with decreasing content of strontium aluminate clinker in the blend. On the contrary the features of hydration products of Portland cement such as the amounts of portlandite, ettringite and CSH gel increase. These results are in agreement with X-ray diffraction analysis (Fig.9), electron microscopy (Figs.8-11) as well as thermal analysis (Fig.12).

Increasing intensity of endothermic effect related to the thermal decomposition of hydrogarnet (Sr_3AH_6, please compare with Fig.5(a) in Chapter 5) at 275 °C and decreasing intensity of the first endothermic peak and its shift to lower temperatures are one of the most expressive features of increasing content of hydration products of PC. The blend of strontium aluminate and Portland cement in the mass ratio of 1:1 shows the highest carbonation as well as portlandite.

The infrared spectrum and thermal analysis show the features of both, calcium carbonate and strontium carbonate. The intensity of DTG peak of calcium (680°C) and strontium carbonate (855 °C) reflects the composition of the blend. The solid state synthesis of strontium aluminate (Eq.43 in Chapter 4) turns the effect on DTA to exothermic, while sole thermal decomposition of calcite is naturally the endothermic process.

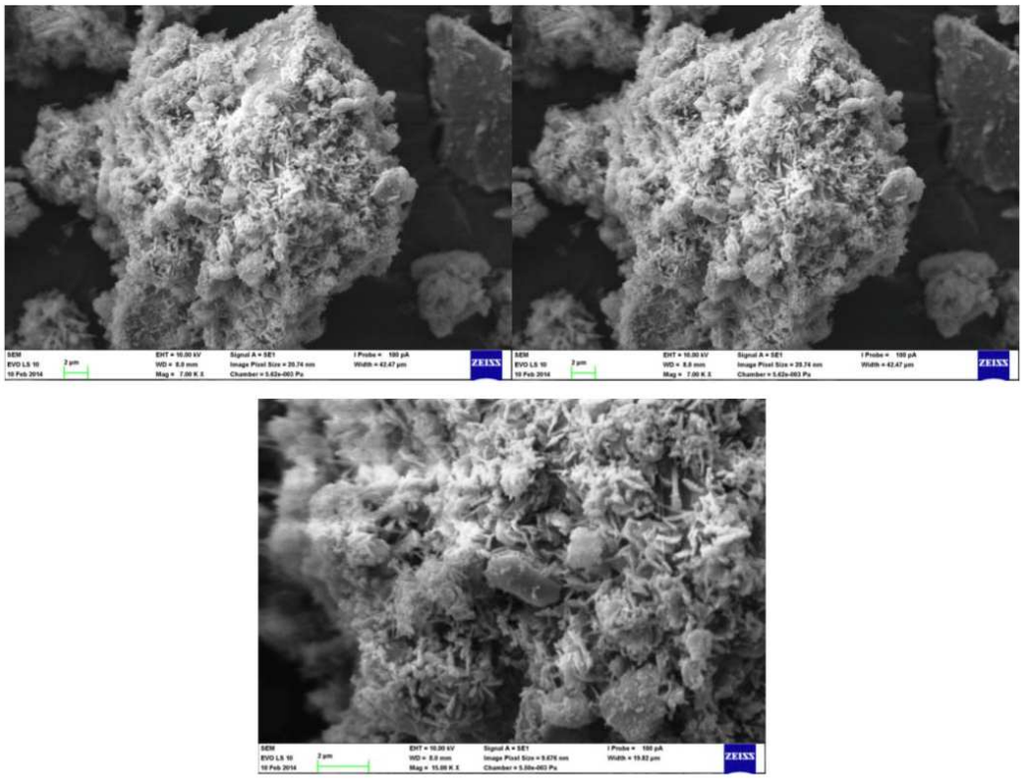

Figure 11. The hydrated cement stone prepared from the mixture of SrAC and PC (1:3).

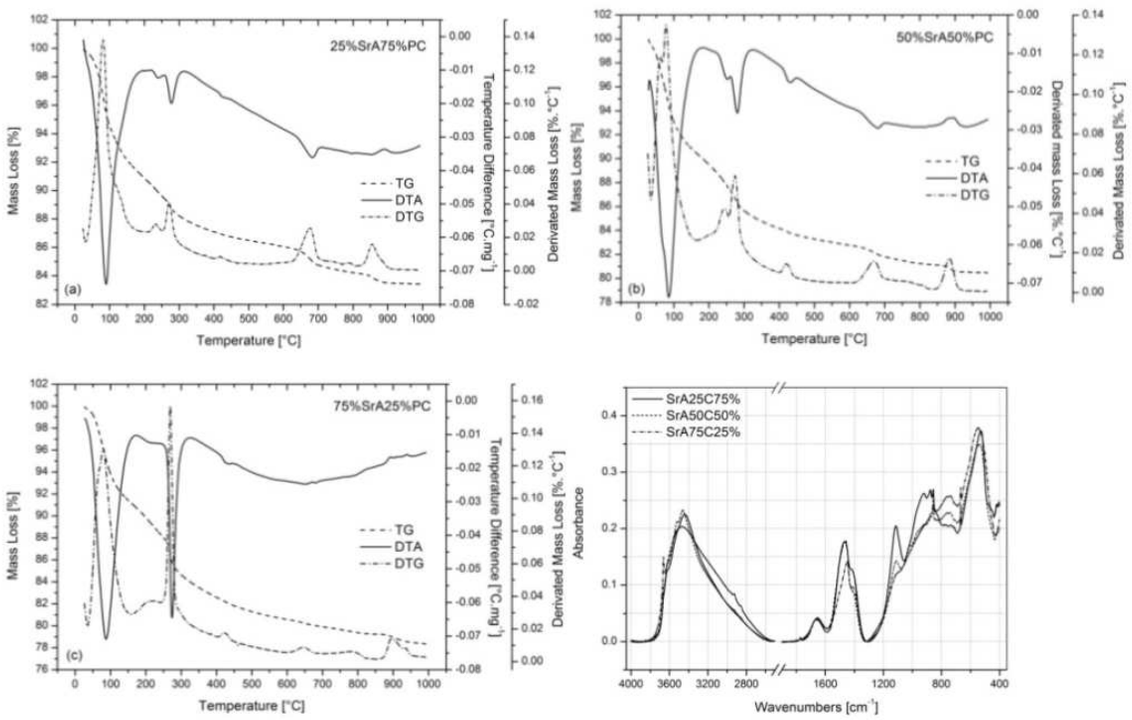

Figure 12. Thermal analysis (a-c) and infrared spectroscopy (d) of hydrated SrA – PC blend.

2. Multicomponent cements

The addition of strontium aluminate cement into calcium aluminate cement increases the time of hydration period and slows-down the rate of heat release (Chapter 7.1.1). It may be useful in order to avoid possible overheating of large constructions caused by setting calcium aluminate cement. The possibility of the preparation of multicomponent cements with admixtures (Fig.1) of pozzolanic materials (microsilica (MS) and metakaolinite (MK)) and latent hydraulic materials such as blast furnace slag (BS) are discussed in this chapter.

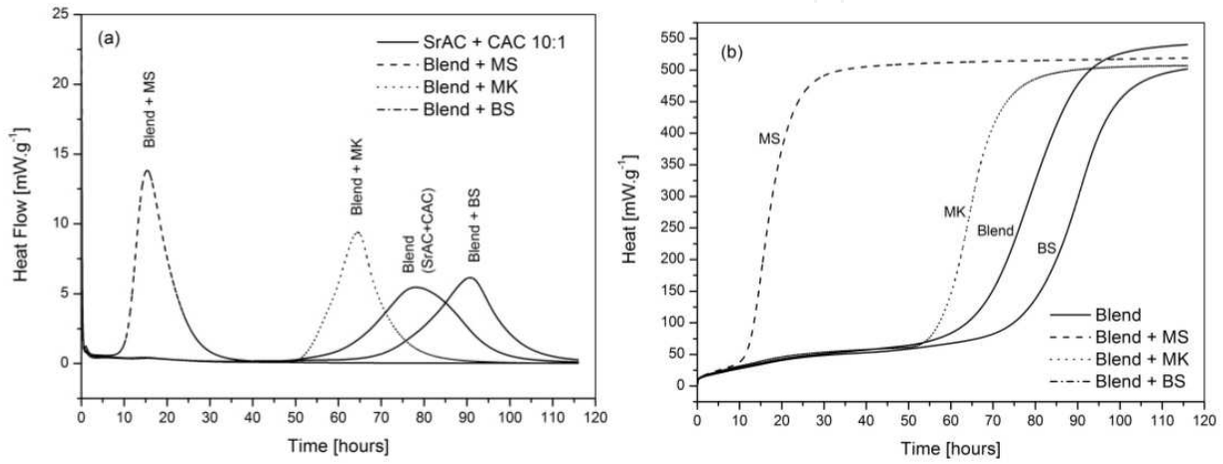

Figure 13. Heat flow (a) and heat of hydration (b) released from the multicomponent cement during the first 128 h of hydration from the blend of CAC and SrC (1:10) with microsilica (MS), metakaolinite (MK) and blast furnace slag (BS).

Isothermal calorimetry performed with the blends of strontium-, calcium aluminate cement containing the materials mentioned above is shown in Fig.13. The main hydration effect of the mixture SrAC and CAC without mineral admixture (NA) started after 50 hours from mixing with water, the heat flow from hydrated sample reached the maximum after 78 hours and was asymptotically falling to the baseline till the 110th hour of hydration. The heat flow from hydrated sample was 0.11 mW g^{-1} after the 115th hour of hydration.

The highest heat flow was measured for microsilica. Microsilica also significantly accelerated the occurrence of the main hydration effect, which began at 7.5 h after mixing with water. The main hydration effect reached the maximum at the time of 15 h and was falling down to the baseline till the 40th hour of hydration. The heat flow from hydrated sample was 0.04 mW g^{-1} after the 115th hour of hydration.

Metakaolinite also increased the heat flow release from the sample and the maximum rate of hydration (64 h). Although the main hydration effect started almost at the same temperature as for the mixture without mineral admixture, it was dropping down to the baseline much faster. Total hydration heat was almost the same for all multicomponent cements (Fig.13 (b)), however, metakaolinite accelerated the hydration of the SrAC-CAC blend. The heat flow from hydrated sample was 0.02 mW g^{-1} after the 115th hour of hydration.

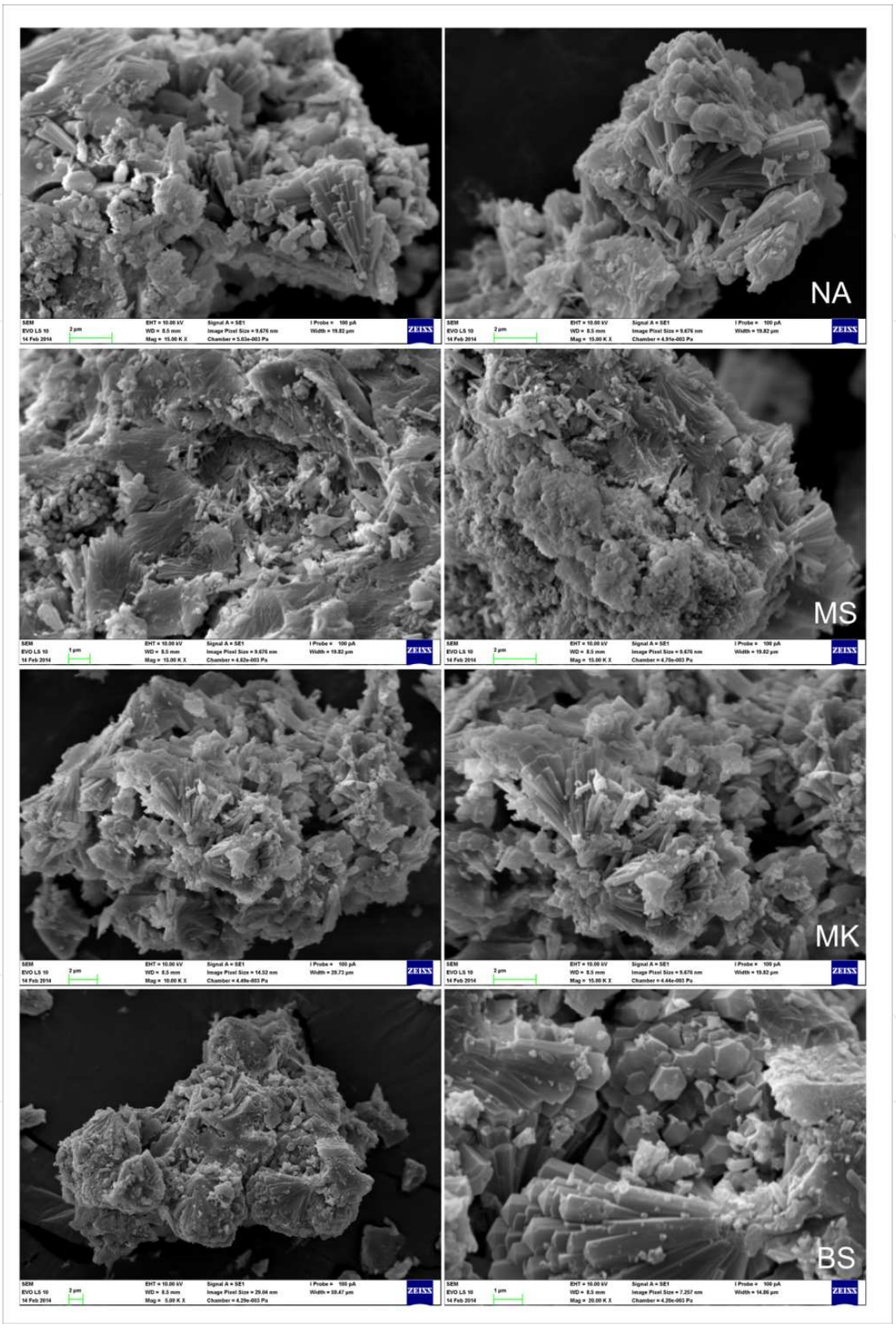

Figure 14. SEM images of hydrated cement stones consisting of CAC+SrA blend (10:1) with 10 % of microsilica (MS), metakaolinite (MK) and blast furnace slag (BS).

The main hydration effect of multicomponent cement with blast furnace slag arises 60 hours after mixing with water. The maximum of the heat flow peak was slightly higher, but it was delayed in comparison with the blend without mineral admixture. The peak was dropping to the baseline till the time of 115 hours after mixing with water. The heat flow from hydrated sample was of 0.27 mW g^{-1} after the 115th hour of hydration.

The effect of mineral admixture on the hydration of multicomponent cements should be expressed as follows:

- Heat flow peak height: MS >> MK >> BS > NA.
- Length of induction period: BS > NA > MK >> MS.

Electron microscopy of hydrated cement stones shows the formation of CSH_{10}, the shape of which is well developed in the sample containing blast furnace slag (BS) and in the blend of calcium-and strontium aluminate cement without mineral admixture (NA).

3. Effect of substitutions on the properties of strontium aluminate cements

The ionic substitutions in the structure of strontium aluminate as the main hydraulic phase of SrAC can induce some modifications in the structure, reactions and properties. As was mentioned in Chapter 1, Sr can partially replace Ca in numerous metal oxides. Therefore, it is often possible to synthesize single-phase mixed oxides, which change the reactivity with water and the setting behaviour of clinker phases or can be used for the preparation of multicomponent cements (described in Chapter 7.2).

There is a complex distribution of Ca and Sr over available sites in $Ca_{3x}Sr_xAl_2O_6$ (where $0 \leq x \leq 3$), but this distribution is not present in hydrated materials where only single Ca/Sr site exists. Therefore, the reaction proceeds by the dissolution of oxide and by the precipitation of corresponding hydroxide at crucial concentration. Since the solubilities of Ca and Sr compounds are likely to be different (in general Ca salts are more soluble), the precipitation of Sr hydroxide will commence prior to that of Ca hydroxide. In the other words, the hydration reaction is not a topotactic reaction. Alternatively, since Ca and Sr occupy different positions in the $Ca_{3x}Sr_xAl_2O_6$ lattice, it is possible that the reaction at Sr-rich phase is favored, preferentially leaching this phase into the solution and favoring the precipitation of Sr-rich hydroxide [8,615].

The investigation of deuterated samples shows that the hydration of mixed calcium-strontium aluminates of the $Ca_{3x}Sr_xAl_2O_6$ type produces a mixture of isostructural (space group of) cubic hydrogarnet phases. The hydrogarnet structure consists of four asymmetric units with the disordered Ca/Sr cations occupying one site within a distorted cube. These cations are displaced so that there are four short and four somewhat longer M-O distances. Al has approximately octahedral environment. In general, the Al-O distance (and the lattice size) in-

creases slightly as the Sr content increases. The difference is however relatively small, the distance increases from 1.910 to 1.945 Å [8].

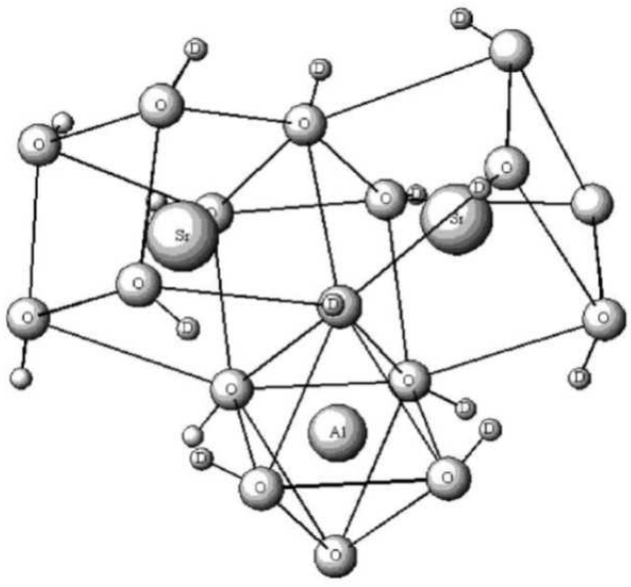

Figure 15. Structure of AlO_6 octahedra and dodecahedra according to Prodjosantoso [8].

The formation of two or three new phases from the initial single-phase oxides, suggests that these new phases may be a miscibility gap in the $Ca_3Al_2(O_4H_4)_3$-$Sr_3Al_2(O_4H_4)_3$ series. Once formed, mixed metal hydroxides seem to be stable and there is no suggestion of Ca^{2+}/ Sr^{2+}ions exchange [8,416,615].

Strontium can also replace calcium in the tetra-calcium aluminoferrite ($Ca_4Fe_2Al_2O_{10}$, C_4AF), which is one of the five major components (~10 %) of Ordinary Portland Cement (OPC) and Calcium Aluminate Cement (CAC). The compound is commonly named according to naturally occurring mineral brownmillerite of similar composition or as ferrite. However, a continuous solid solution $Ca_2Al_xFe_{x-1}O_5$ exists, where $0 \leq \leq 0.7$ and both $Al^{3+}$and Fe^{3+}cations occupy the tetrahedral and octahedral sites. Therefore C_4AF is only a point in this series of solid solution for x=0.5. The end member C_2A, where x=1, can be prepared only at increased pressures of 2500 MPa. The series $x < 0.7$ is not quite isostructural, and the space group changes from to near to $x > 0.33$ [7,12,616-618].

Ordered vacancy perovskite-related type materials such as brownmillerites can be expressed by a general formula $A_2B_2O_5$ or $A_2BB'X_5$ (Fig.16(a)), where B=transition metal cations with octahedral co-ordination and B′=transition metal cations with tetrahedral coordination. The materials adopting the brownmillerite structure consist of a single B cations or of two different B cations, which are commonly disordered over both octahedral and tetrahedral sites or may be ordered according to the preference of transition metal cations for a particular co-ordination environment [619]. The oxygen nonstoichiometry of brownmillerite also changes with the oxygen partial pressure and the temperature [618,620-622].

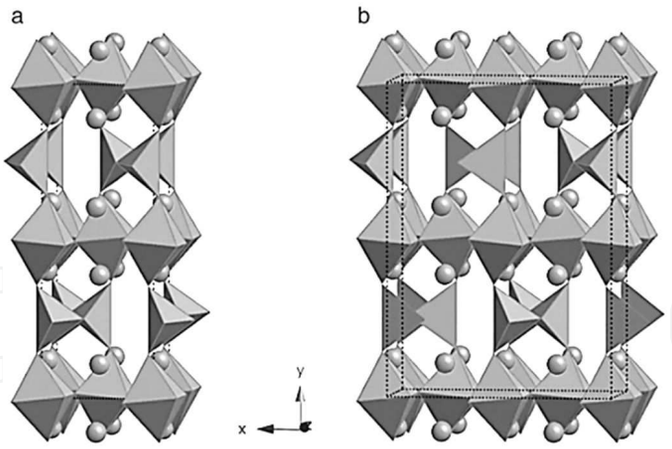

Figure 16. The conventional chain-ordered Ibm2 structure (a) and the Pbma supercell (b) of $Sr_2Fe_2O_5$ [622].

The brownmillerite structure can be explained by removing ½ of the oxygen atoms from the layer of the cubic perovskite-type structure, consisting of octahedra, creating vacancies along the [110] direction. Corner-sharing BO_6 octahedra alternates with layers of $B'O_4$ tetrahedra arranged in chains parallel to (100) direction. The crystal structure can be described as a sequence of B′–BB′–B–B′–B parallel to (010) direction. Cations A are required for the charge compensation and they occupy voids between $BO^{6-}$and $B'O^{4-}$polyhedra. Cations A are coordinated by 8 oxygen neighbours forming a distorted bicapped trigonal prism. The presence of 'channels' of oxygen vacancies between these chains allows some brownmillerites and their derivatives to display ionic conductivities comparable to the stabilized zirconia systems [618,622,623].

The displacement of tetrahedral B and O ions from their ideal positions upon the formation of brownmillerite from the parent perovskite gives rise to two opposite orientations for the tetrahedral chains, which can be assigned 'left' (L) and 'right' (R) [621,624].

The symmetry of brownmillerite is thus determined by the distribution of L-and R-chains in the structure, with three commonly recognized configurations [622]:

i. Pure L (or R), resulting in the *Ibm2* space group (Fig.16(a));

ii. Complete L/R disorder (Icmm);

iii. Strict alternation of L and R layers along b direction (Pcmn).

The brownmillerite structure type of mixed ionic/electronic conductor $Sr_2Fe_2O_5$ has been well-established since 1970s [625]. Although the diffraction studies of $Sr_2Fe_2O_5$ have clearly established a body-centered unit cell, the assignment of either the Icmm or models to describe the tetrahedral chain arrangement has varied among experiments [626]. Electron diffraction (ED) images revealed the evidence for short-range $Sr_2Fe_2O_5$ superstructures defined by complex ordering patterns of L and R chains (Fig.17) both within and between the tetrahedral layers [627]. Single crystal neutron diffraction revealed a supercell (Fig.16(b)) with a doubled axis (space group), compared to the conventional model containing disordered left-

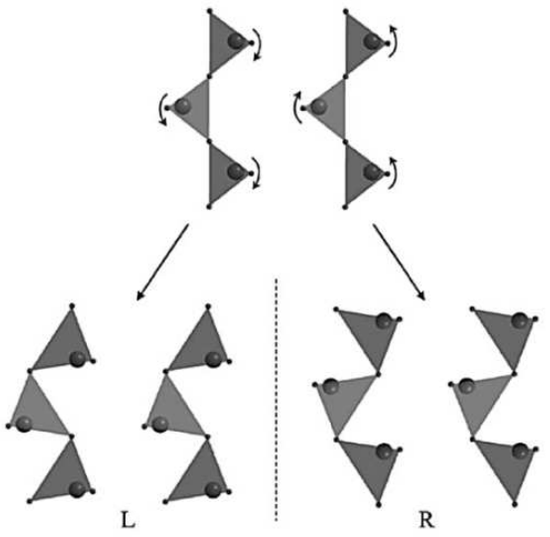

Figure 17. Cooperative twist yields to left or right-handed chains [624].

and right-handed tetrahedral chains. Therefore, the model conventionally used to describe the local chain order of $Sr_2Fe_2O_5$ is incorrect [622].

Transition brownmillerite phases $Ca_{1-x}Sr_xFe_{2.5+\delta}$ where $0.3 \leq x \leq 0.7$ are studied predominantly due to their promising applications in electrochemical devices at high temperature such as ceramic membranes for oxygen separation, electrodes of solid oxide fuel cells (SOFCs), electro- and photocatalysts, battery electrodes and sensor materials, etc. [620,622,628,629,630]. The transition brownmillerite phases with the composition of $La_{1-x}Sr_xCo_{0.8}Fe_{0.2}O_{3-\delta}$ can be prepared under low partial pressures of oxygen, where the value of > 0.7 [629].

The $LaACuGaO_5$, where A=Ca, Sr, brownmillerite system consists of alternating layers of corner-sharing CuO_6 octahedra and GaO_4 tetrahedra stacked along the long axis, with La and A cations statistically occupying the 10-fold cavities within the structure [619,631,632]. Anion-vacancy ordered 'triple layer' structure, related to the brownmillerite structure by the insertion of an additional layer of octahedra has the composition $LaCa_2Fe_2GaO_8$ [633].

Mn-containing brownmillerites ($A_2MnBO_{5+\delta}$, where A=Ca, Sr and B=Ga, Al) may be perspective compounds as low-field CMR materials. The system $Sr_2MnGaO_{5+\delta}$ (Fig.18) consists of alternating MnO_2 and $GaO_{1+\delta}$ layers (–MnO_2–AO–GaO–AO–MnO_2–AO–GaO–MnO_2–) [619,634-638].

Perovskite oxide with the general formula of ABO_3 is a kind of frequently encountered structure in inorganic chemistry. Its cubic crystal structure is composed of a three-dimensional framework of corner-sharing BO_6 octahedra. $SrFeO_x$ (SFO), where $2.5 \leq x \leq 3.0$, were extensively studied as ferromagnet and antiferromagnet and due to their photocatalytic activity [620,639-641].

Brownmillerite-and perovskite-type compounds exhibit also some serious disadvantages including the thermodynamic instability under large oxygen chemical potential gradients,

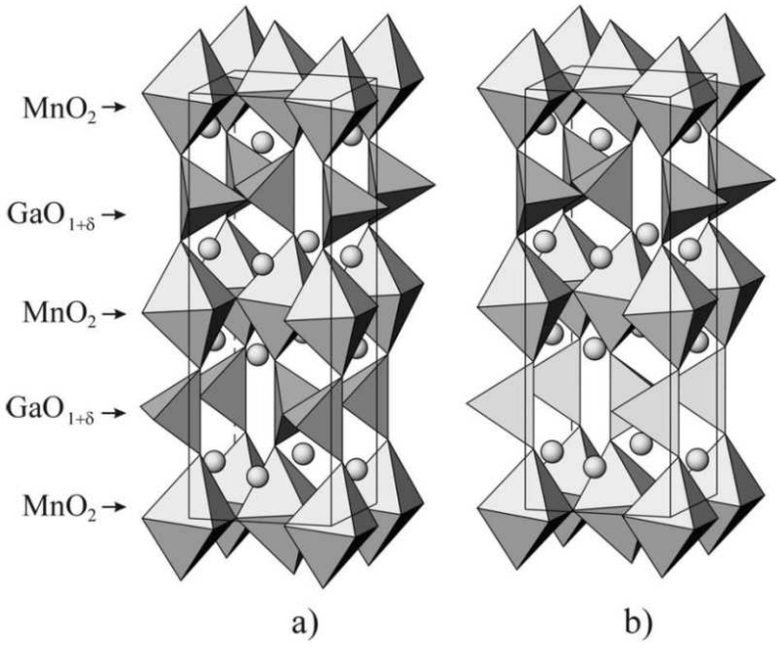

Figure 18. Crystal structure of Sr_2MnGaO_5 brownmillerites with Ibm2 (a) and Pnma (b) space symmetry. Cations are drawn as spheres [638].

poor thermomechanical properties associated with very high chemical and thermal expansion and the reactivity with CO_2 [642].The relation between the orthorhombic brownmillerite and the cubic perovskite-type structure is given as: $a \sim \sqrt{}a_{per}$, $b \sim 4a_{per}$, $c \sim \sqrt{}a_{per}$, where a_{per} is the cell dimension of the cubic perovskite [618].

The protonic conduction was discovered for the brownmillerite-type $Ba_2In_2O_5$ in 1995 by Zhang and Smyth [643] that is related to the formation of $Ba_2In_2O_5$ H_2O hydrate in a humidified atmosphere. Protons bound to oxygen in hydrate cross-links between oxygen [644-646]. In order to improve the proton conductivity it is necessary to stabilize the hydrate compound at high temperature (573 K). The dehydration temperature increases∼50 K due to the substitution of In by Sc, Lu and Y. Since the substitution of In by $M^{3+}$was not possible for $x >$ 0.3 in $Ba_2(In_{1-x}M_x^{3+})_2O_5$ H_2O, further increase in the thermal stability of the hydrate compound by the substitution of In cannot be expected. Tetragonal $Ba_2Sc_2O_5$ and cubic $BaScO_{3-\delta}$ also form hydrates $Ba_2Sc_2O_5 \cdot 0.60H_2O$ and $BaScO_{3-\delta} \cdot 0.37H_2O$, but the dehydration temperatures are even lower than that for $Ba_2In_2O_5$ [647,648].

3.1. Substitution of Al_2O_3 by Cr_2O_3

Cr_2O_3 and Al_2O_3 are sesquioxides having the same corundum crystal structure, which is approximately hexagonal, involving close-packed oxide ions with $Cr^{3+}$and Al^{3+}ions occupying two thirds of available octahedral sites [649,650]. The solid solution ($(Al_{1-x}Cr_x)_2O_3$) obeying **Vegard's law**[2] [651] is formed over the entire range of compositions[3] in Al_2O_3 – Cr_2O_3 sys-

2 Empirical rule that enables to calculate the crystal lattice parameter of solid solution or alloy from the concentration of constituents.

tem. With regard to the positive influence of chromia (Cr_2O_3) on the sintration as well as physical and refractory properties of Al_2O_3 ceramics [652-656], the effect of substitution of alumina by chromia in the strontium aluminate cement was investigated.Cr-doped structures have been widely studied as ceramic pigments [649] and catalyzers [657-659].

Cr_2O_3 is not stable and changes to CrO_3 in an atmosphere in which the oxygen partial pressure is relatively high such as air. CrO_3 exhibits high vapor pressure, so it is difficult to obtain a dense sintered body of Cr_2O_3 in an air atmosphere. In order to obtain a dense sintered body of Cr_2O_3, the sintering should be performed in an atmosphere with low oxygen partial pressure in which Cr_2O_3 remains stable [653].

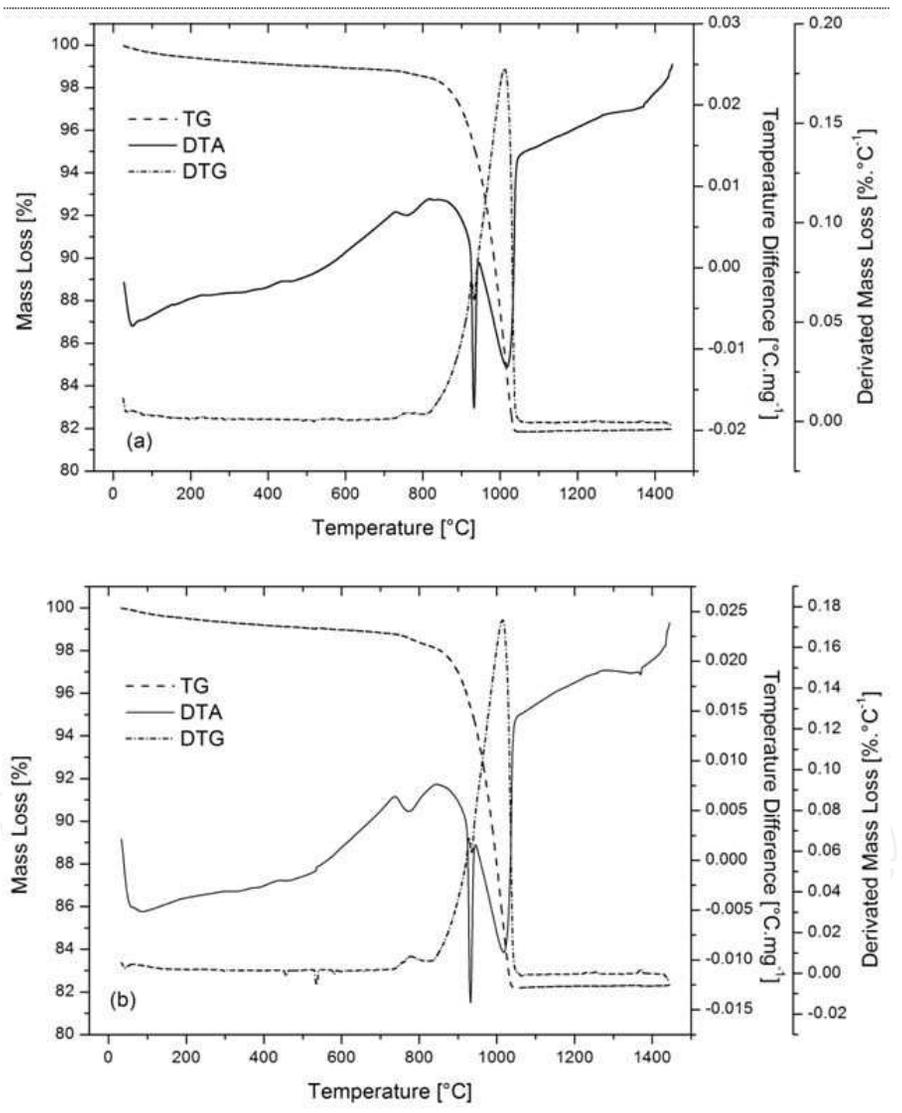

Figure 19. Thermal analysis of clinker prepared with 5 % (a) and 10 % Cr_2O_3 (b).

3 An immiscibility gap is present below 950°C, where two crystalline phases exist (alumina-rich and chromia-rich solid solutions), but the actual decomposition of homogeneous solid solution into two phases proceeds very slowly [651].

The toxicity and the transport behaviour of Cr depend strongly on its valence. The most stable oxidation states in the environment are hexavalent and trivalent. Cr(VI) exists primarily in the form of $HCrO_4^-$(bichromate) and CrO_4^{2-}(chromate), which are strong oxidants and can cause kidney tubule necrosis and, by inhalation, lung cancer. Cr(VI) compounds are typically soluble in groundwater, and thus mobile and bioaccessible. Where the intermediates to low redox potentials exist, Cr(VI) can be reduced to Cr(III) which usually forms insoluble oxides and oxyhydroxides being less bioaccessible [660].

Thermal analysis of raw materials with the substitution of 5 and 10 % Al_2O_3 by Cr_2O_3 (Fig. 19) shows increased intensity and peak temperature (from 735 to 785 °C) of endothermic process, which is probably related to the formation of chromia spinel phase. To compare with raw material without chromia (Fig.23 in Chapter 4), there is sharp transformation effect of α-$SrCO_3$ to β-$SrCO_3$ (please compare with Fig.12 in Chapter 4). It is possible to use the thermolysis of mixed alums in order to prepare mesoporous chromia-alumina [661] as pure and high reactive precursor for the synthesis. That may lead to the assumption that the addition of Cr_2O_3 into the raw meal suppresses the decomposition of strontium carbonate and leads to less reactive clinker containing the sintering additive (similarly to the effect described in Chapter 6.1.4).

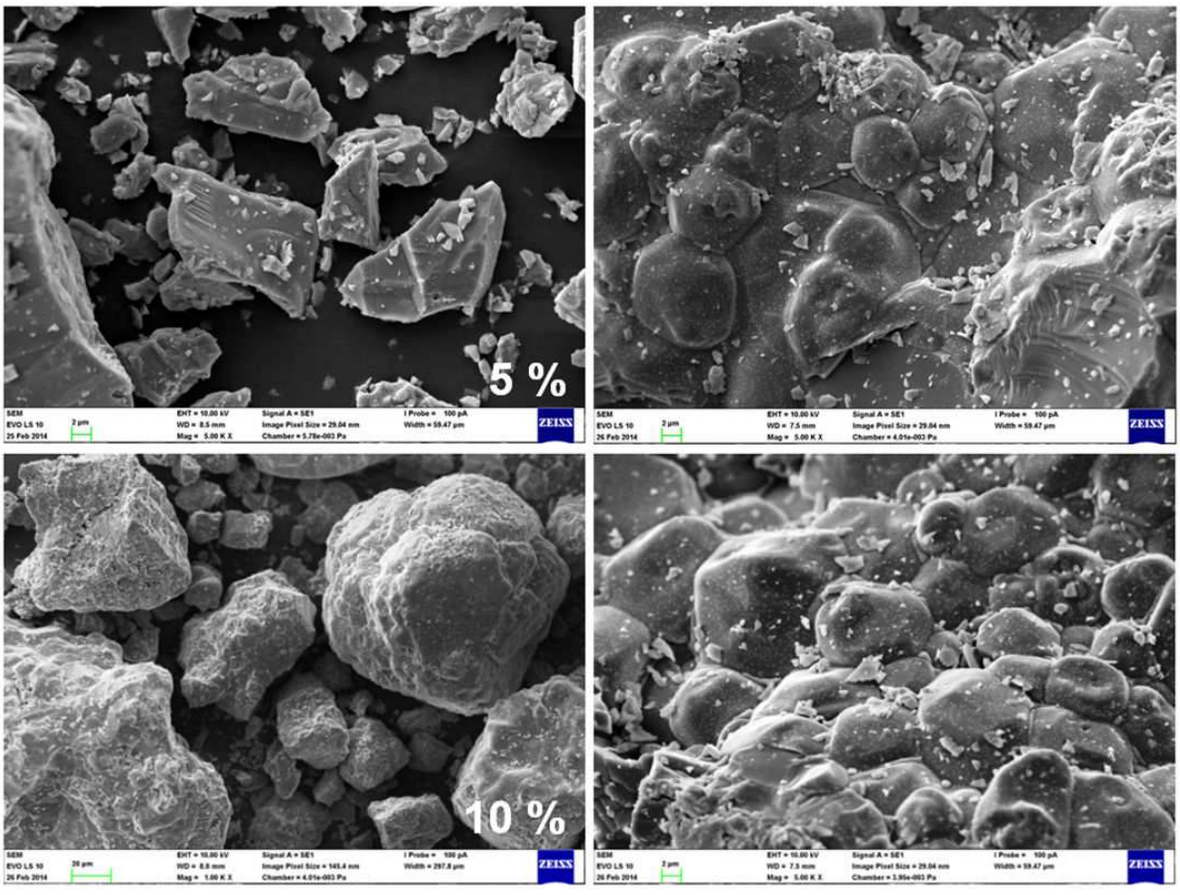

Figure 20. Scanning electron microscopy of clinker prepared with 5 % (a) and 10 % Cr_2O_3 (b).

The addition of Cr_2O_3 in to the raw meal leads to the formation of tetragonal strontium oxide chromate ($3SrO \cdot 3Al_2O_3 \cdot SrCrO_4$) [662] and strontium hexaaluminate causing the detriment of strontium aluminate as the main clinker phase (Fig.21). This endothermic process should be described by the following reaction:

$$8\,SrCO_3 + 6\,Al_2O_3 + Cr_2O_3 + 3/2\,O_2(g) \rightarrow 2\,(3SrO \times 3\,Al_2O_3 \times SrCrO_4) + 8\,CO_2(g) \quad (3)$$

The lack of SrO supports the formation of strontium hexaaluminate.

That behaviour also enables to explain the missing effect related to the formation of strontium aluminate, which is formed at higher temperature probably via the diffusion of Al^{3+}ions through Cr_2O_3-Al_2O_3 layer of formed solid solution. The opposite model, in which the spinel layer would be formed on Cr_2O_3 particles cannot explain the suppression of the formation of strontium aluminate revealed from the TG-DTA experiment.

$3SrO \cdot 3Al_2O_3 \cdot SrCrO_4$ is a pigment with hexavalent chromium and provides prepared clinker with yellow-greenish color. Since the transformation temperatures and the temperatures of endothermic effect are the same for both samples, increasing content of Cr_2O_3 seems to have no influence on the thermal decomposition of strontium carbonate (after the formation of layer on the surface of $SrCO_3$ grains the increasing abundance of Cr_2O_3 doesn't have any effect).

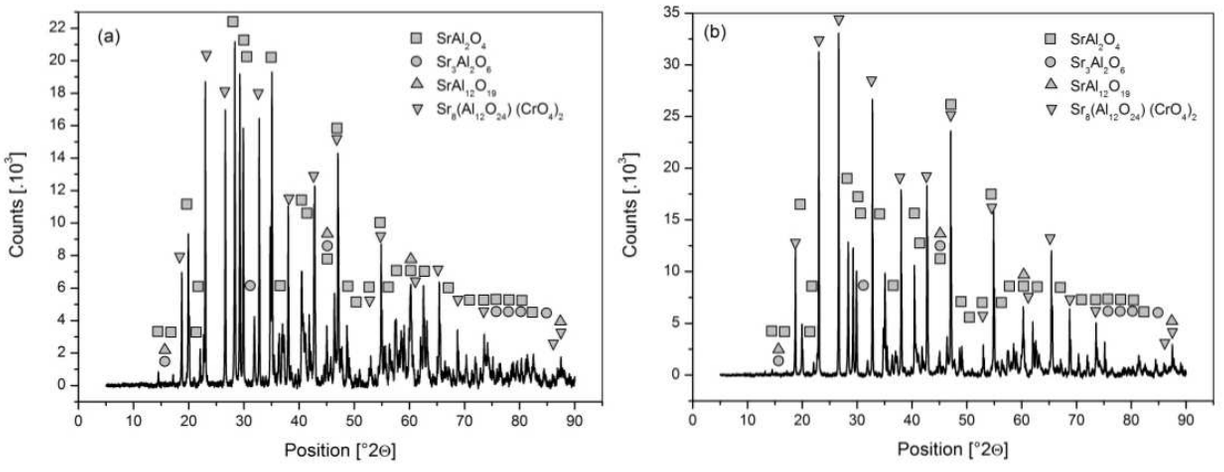

Figure 21. XRD analysis of strontium aluminate clinker doped by chromia.

The raw meal was treated to the temperature of 1500 °C under static air and ground after cooling. Scanning electron microscopy of ground clinker shows the formation of globular aggregates of rounded particles with the surface showing intersections of spherical shapes, which are better developed in the sample prepared with 10 % of Cr_2O_3 (Fig.20). Ground particles show brittle fracture through the glassy-like phase of clinker particles.

The diffraction lines of strontium oxide chromate ground clinker prepared with 10 % of chromia reaches even higher intensity than strontium aluminate. The amount of formed

SrA_6 phase seems to be decreasing with increasing content of Cr_2O_3 in the raw meal. Considerable amount of formed phases without hydraulic activity leads to the conclusion that the raw meal containing chromia should be prepared in slightly reducing atmosphere.

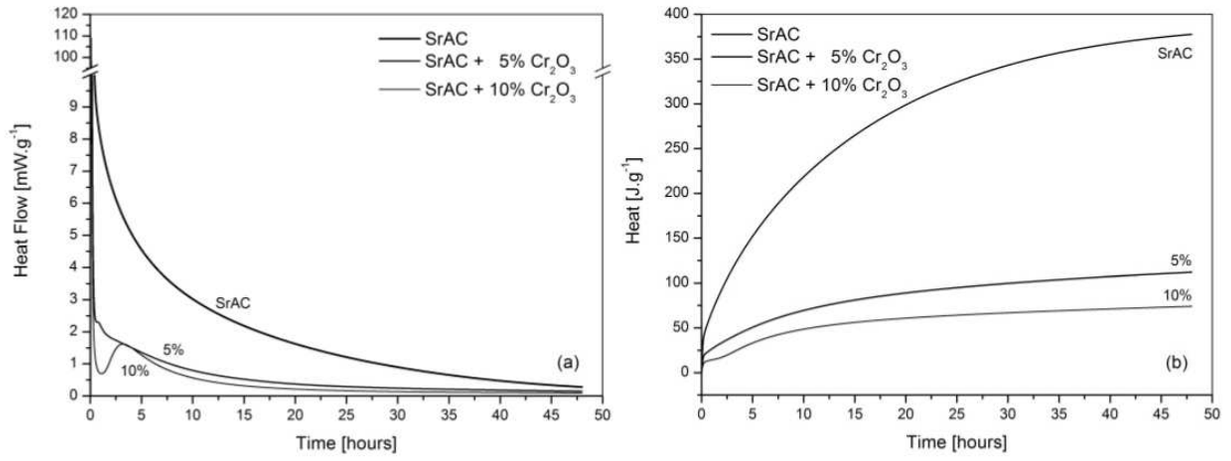

Figure 22. Heat flow (a) and heat of hydration (b) for the samples doped with chromia.

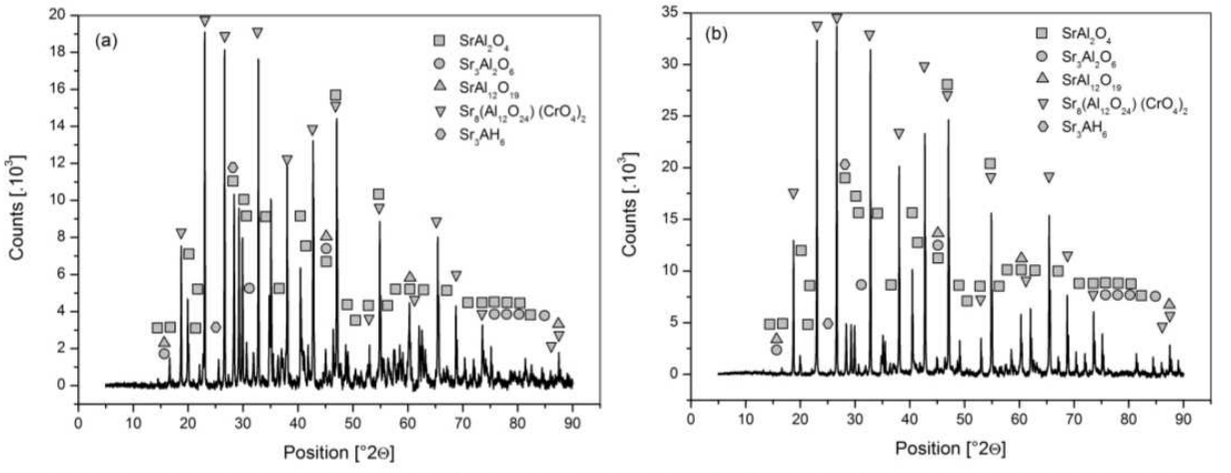

Figure 23. XRD analysis of strontium aluminate clinker after hydration.

The influence of the substitution of Al_2O_3 by Cr_2O_3 on the properties of strontium aluminate cement was investigated by isothermal calorimetric measurement of hydration at 25 °C (Fig.22).

The results show that the introduction of Cr_2O_3 into the structure of SrA significantly reduces the hydraulic activity and leads to the appearance of induction period. That behaviour is probably caused by the formation of chromium spinel (please see Chapter 10.12).

This behaviour results from decreasing content of strontium aluminate in the clinker with increased amount of added chromia. That means that newly formed phase of strontium alu-

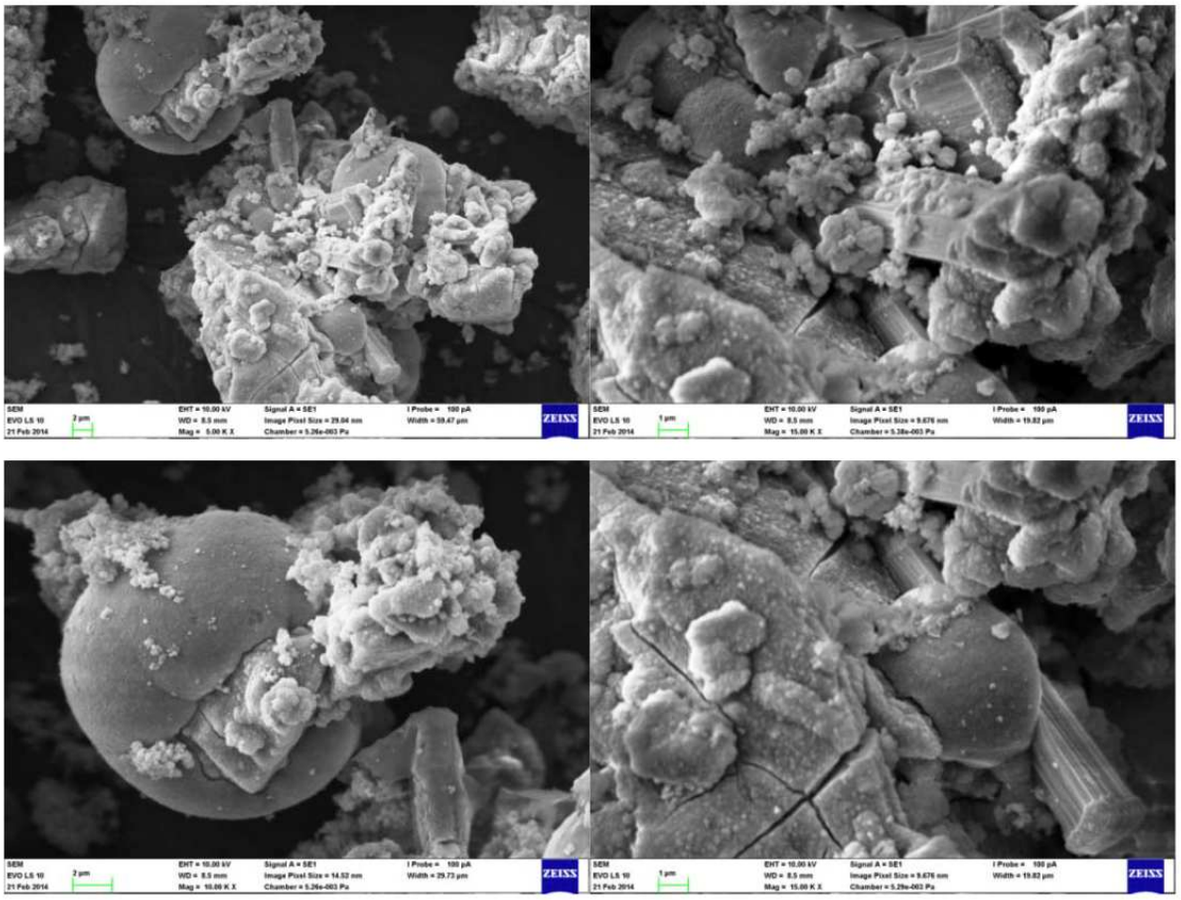

Figure 24. SEM images of hydrated cement stone for the sample prepared with 5% of Cr_2O_3.

minium oxide chromate has no hydraulic activity. X-ray diffraction analysis of hydrated cement stone supports the conclusion that strontium oxide chromate does not show significant hydraulic activity, if any. The main product of hydration remains tri-strontium aluminate hexahydrate as for the clinker prepared without chromia and the intensity of diffraction lines of strontium oxide chromate is not changed.

Electron microscopy shows that the morphology of hydration product is different from strontium aluminate cement without the addition of Cr_2O_3 into the raw meal (Fig.6 in Chapter 5). Moreover, the external appearance of hydrates changes with the amount of added chromia. Long columnar crystals, typical for the sample prepared with 5 % of Cr_2O_3 (Fig.24) are not present in the hydrated cement stone prepared from ground clinker with 10 % Cr_2O_3 (Fig.25). With increasing content of Cr_2O_3 the size of spheres was also significantly reduced.

3.2. Substitution of Al_2O_3 by Fe_2O_3, B_2O_3 and Y_2O_3

Strontium aluminate cements with the substitution of 5 % of Al_2O_3 by Fe_2O_3, B_2O_3, Y_2O_3, V_2O_5, ZrO_2, MnO_2 and ZnO were prepared in order to evaluate the influence of these compounds on the behaviour during hydration. The samples were pelletized and thermally

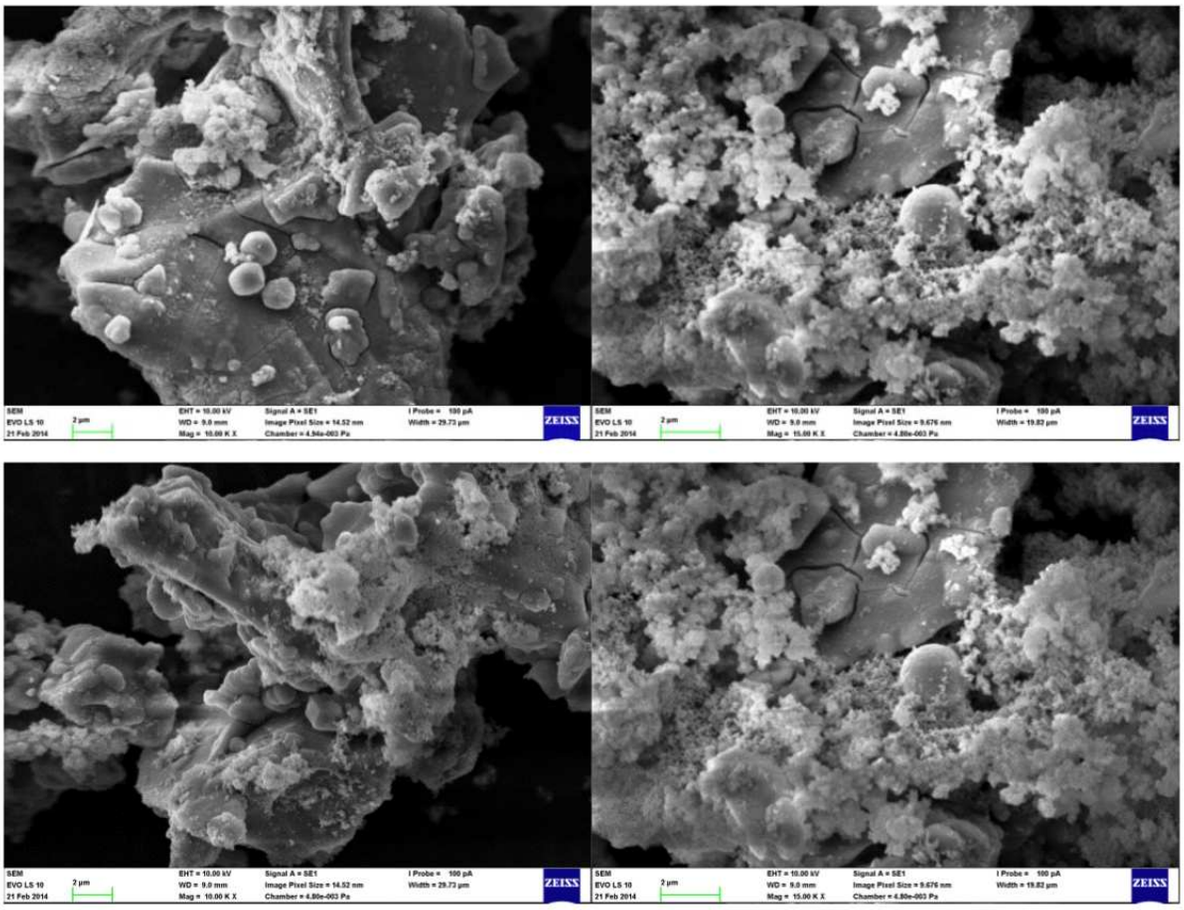

Figure 25. SEM images of hydrated cement stone for the sample prepared with 10 % of Cr_2O_3.

treated to the temperature of 1500 °C (1 hour). The thermal analysis of raw materials upon thermal treatment is shown in Fig.26.

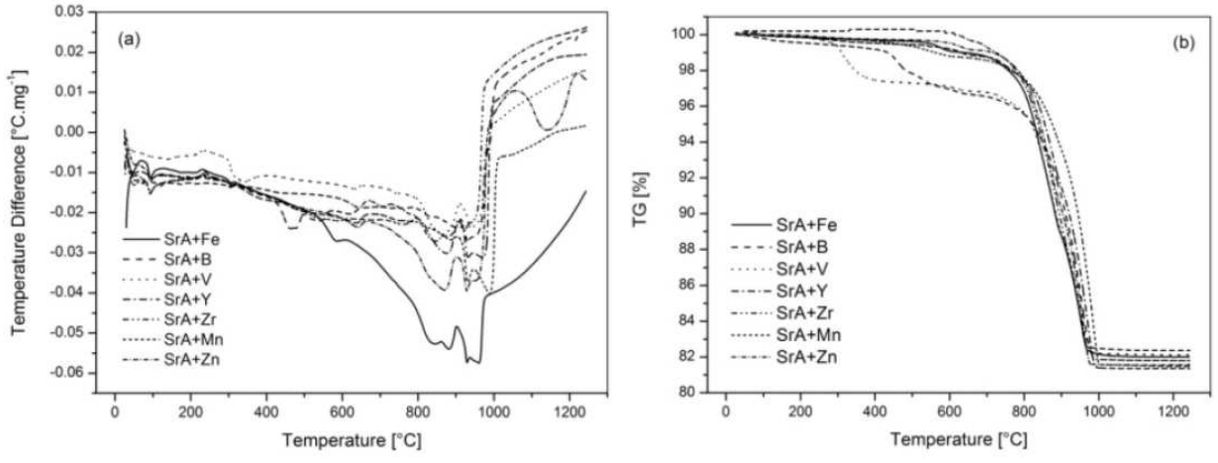

Figure 26. Thermal analysis of raw meals heated at the rate of 10 °C min^{-1}: DTA (a) and TG (b).

All investigated samples show almost the same mass loss of 8 %. The major part of mass loss is caused by the thermal decomposition of strontium carbonate that takes place within the temperature range from 700 to 1 000 °C.

Dopant element	Mechanism		R^2	E_a	A
	$g(\alpha) = kt$	Abr.		[kJ·mol^{-1}]	[s^{-1}]
Fe	-ln (1-α)^3	A_3	0.9925	583.06	$3.04 \cdot 10^{23}$
B	1-(2α/3)-(1-α)$^{2/3}$	D_4	0.9996	379.56	$3.79 \cdot 10^{12}$
V	-ln (1-α)^3	A_3	0.9911	664.46	$7.07 \cdot 10^{26}$
Y		A_3	0.9941	613.93	$1.54 \cdot 10^{24}$
Zr		A_3	0.9976	611.70	$5.28 \cdot 10^{24}$
Mn	1-(1-α)$^{2/3}$	$F_{1/3}$	0.9977	169.61	$8.13 \cdot 10^{3}$
Zn	-ln (1-α)^3	A_3	0.9922	613.93	$3.74 \cdot 10^{24}$

Table 1. Influence of dopants on the thermal decomposition of strontium carbonate.

There is a significant difference compared to the sample prepared with the addition of chromia (Chapter 7.3.1) since the intensive exothermic peak related to the synthesis of strontium aluminate arises for all samples. On the contrary, this peak is smaller for the sample prepared with B_2O_3.

The model fitting method (Chapter 1.6.1) applied to the TG results provides the kinetic data listed in Table 1. The kinetics of thermal decomposition of strontium carbonate is changed by the presence of dopants (please consult with the results in Chapter 4.2). It can be seen that Fe, V, Y, Zr and Mn have similar effect on the mechanism (random nucleation) and kinetics of thermal decomposition of $SrCO_3$. The addition of B_2O_3 changes the mechanism to the non-steady state 3D diffusion and MnO_2 leads to the process driven by the rate of chemical reaction of one-third order.

The admixtures lead to the decreasing intensity of strontium aluminate diffractions (Fig. 27(a)) in the clinker after the thermal treatment. Based on this effect, they can be ordered as follows:

$$B_2O_3 > ZnO > MnO_2 > ZrO_2 > Fe_2O_3 > Y_2O_3 > V_2O_5.$$

The shift of the most intensive diffraction lines of $SrAl_2O_4$([-211], [220] and [211], Fig.27) for the samples prepared with ZnO and Fe_2O_3 indicate the substitution of $Zn^{2+} \leftrightarrow Sr^{2+}$and $Fe^{3+} \leftrightarrow Al^{3+}$, respectively. While, the clinker prepared with ZnO shows well developed $SrAH_6$ crystals in hydrated cement stone (Fig.29), the clinker doped with Fe_2O_3 exhibits the highest heat released upon hydration (Fig.28).

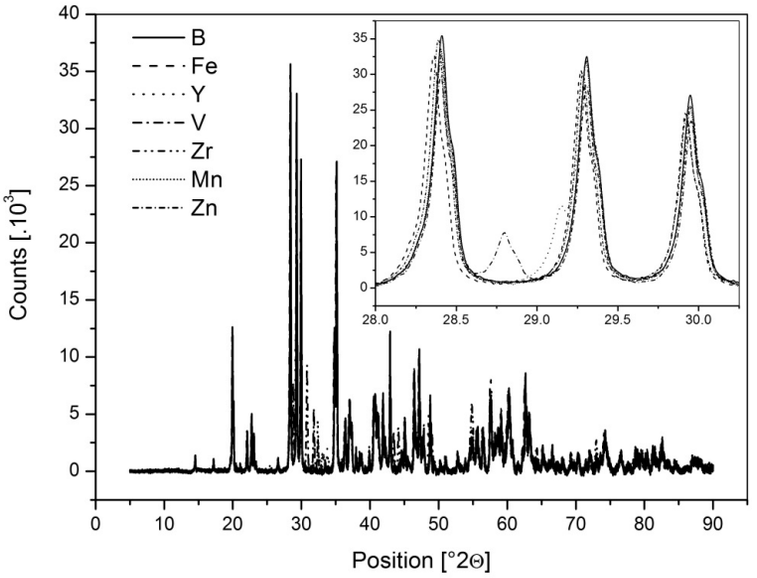

Figure 27. X-ray analysis of strontium aluminate clinker prepared with dopants before hydration.

Observed influence of B_2O_3 on the synthesis and hydration (Fig.28) of strontium aluminate clinker is caused by the ability to incorporate BO_4 unit into the framework of $SrAl_2O_4$ instead of AlO_4 tetrahedra [663]. $(BO)_4$ tetrahedra are of more ionic nature than $(AlO)_4$ due to smaller size ($r_{B3+} < r_{Al3+}$) and higher electronegativity (X_B=2 and X_{Al}=1.6, Pauling´s scale) of boron [377,664]. B_2O_3 is also known as a glass former, which has low melting point around 460 ◦C. It is regarded as an excellent flux to facilitate the material diffusion (pleasse see Table 1). Thus, B_2O_3 is usually added in the preparations of $SrAl_2O_4$ in order to reach lower forming temperature [663].

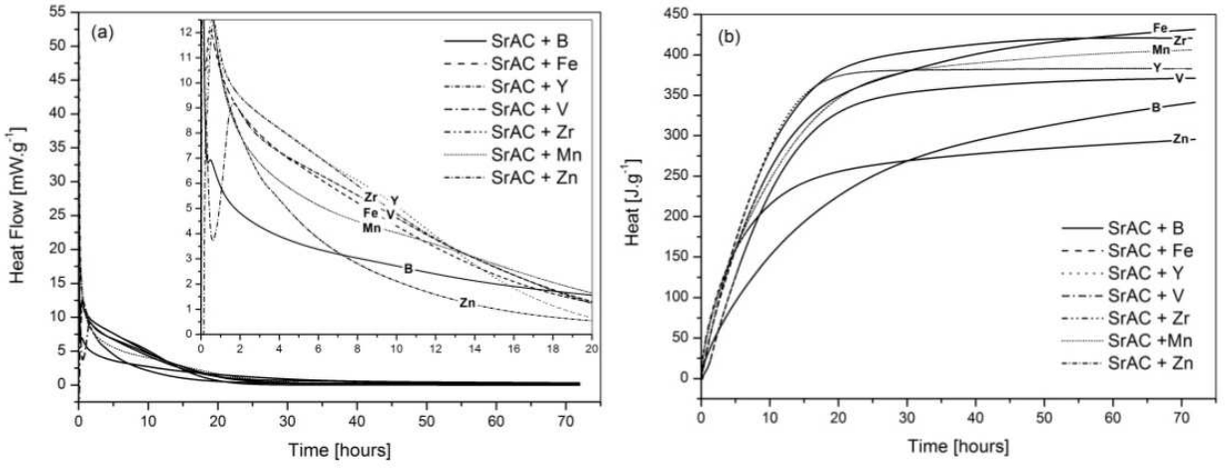

Figure 28. Hydration of clinker prepared with dopants.

The hydration of prepared samples was investigated by isothermal calorimetry at the temperature of 25 for the first 72 h of hydration (Fig.28). Since there is no induction period and large amount of heat is released immediately after mixing with water, the course of hydration of clinkers doped with ZnO and MnO_2 is similar to that of pure strontium aluminate. The heat flow then asymptotically decreases to the baseline. According to the decreasing heat of wetting, the samples can be ordered as follows:

$$ZnO >> MnO_2 > B_2O_3 > Fe_2O_3 \approx Y_2O_3 > ZrO_2 >> V_2O_5$$

Other clinkers show the induction periods the lengths of which decrease with following dopants applied:

$$V_2O_5 >> ZrO_2 > Fe_2O_3 > Y_2O_3 >> B_2O_3.$$

According to the time of maximum of main hydration peak and its height, the samples should be ordered as follows:

- Time: $V_2O_5 >> ZrO_2 \approx Y_2O_3 \approx B_2O_3 > Fe_2O_3$.
- Intensity: $Y_2O_3 \approx ZrO_2 \approx Fe_2O_3 > V_2O_3 > B_2O_3$.

Electron microscopy of hydrated cement stone (Fig.29) shows the formation of globular (grape-like) aggregates. But also the formation long columns of layered aggregates (*a, b* and *c*), long needle-like crystals (*b*) and well developed $SrAH_6$ crystal (*g, h*) can be observed. The stacked columnar structure of gibbsite aggregate indicates the option to use doped strontium aluminate cement for the preparation of iron-and aluminium based double layered hydroxides (LDH [665-672]).

Figure 30(a) describes typical Raman spectrum of pure monoclinic $SrAl_2O_4$, where the main peak at 467 cm^{-1} belongs to bending of O-Al-O in [AlO_4] tetrahedra [795,1009]. The partial substitutions of Al_2O_3 and $SrCO_3$, as the reactants in solid state reaction with different metal oxides lead to theformation of new phases as is indicated by the shifts of the main peak of [AlO_4] tetrahedral (Fig.30(b)).

The significant shifting was observed for the structure doped with MnO_2 and should be described as the distortion of monoclinic lattice structure. The experimentally determined influence of various metal oxides in lattice shift is ordered as follows:

$$MnO_2 > ZnO > B_2O_3 > Y_2O_3 > ZrO_2 > pure\ \ SrA\ \ phase > V_2O_5 > CaO.$$

Increasing content of boron in prepared clinker leads to the formation of large hexagonal plates during hydration (Fig.31). According to EDX (Energy Dispersion Spectroscopy), the composition of these crystals corresponds to Sr_2AH_x. The formation of well developed crystals of Sr-analogue of $C_2AH_8$was observed only for the samples doped by high amount of boron.

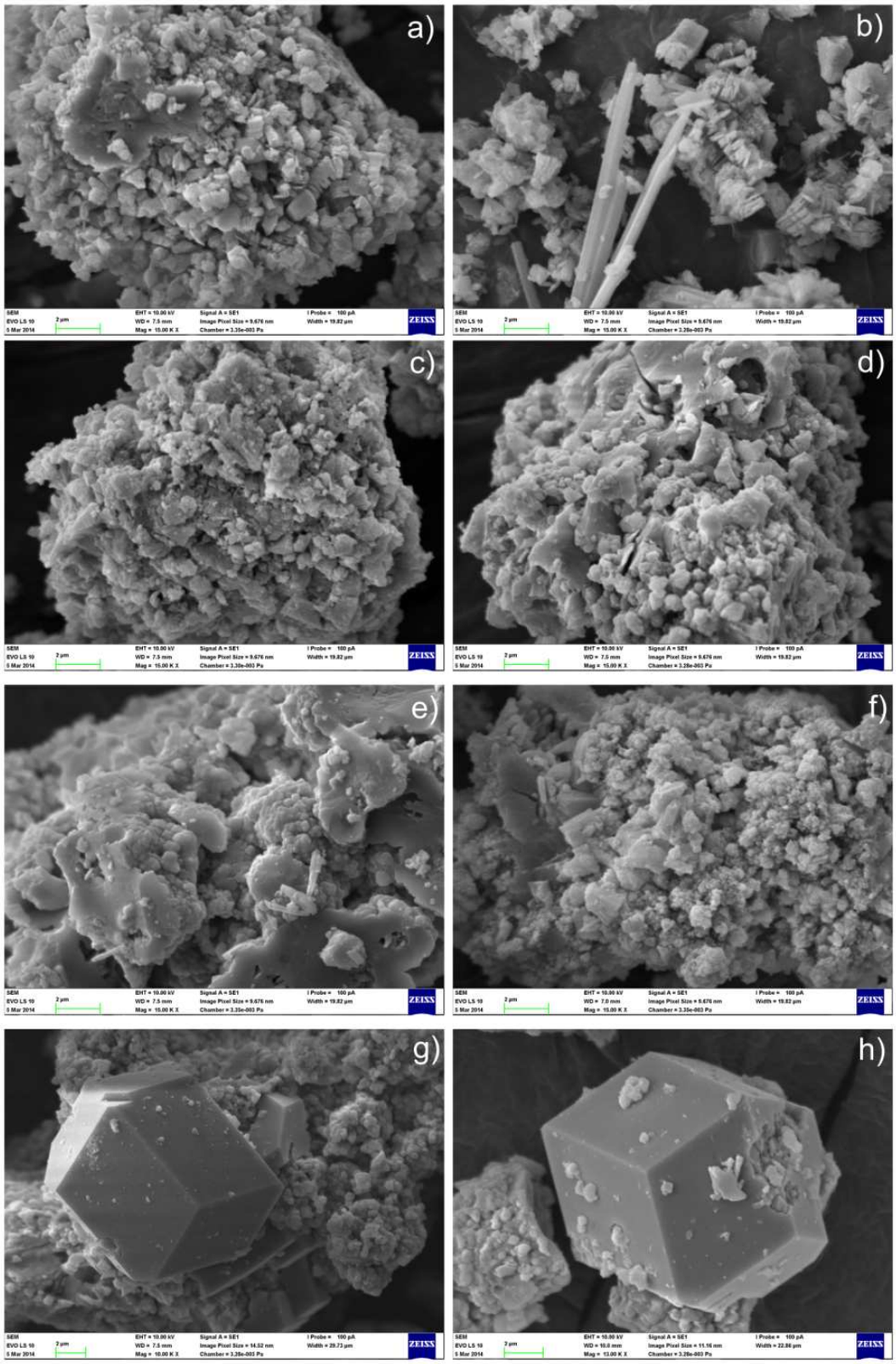

Figure 29. Electron microscopy of hydrated cement stone of clinker prepared with 5 % of B_2O_3(a), Fe_2O_3 (b) Y_2O_3(c), V_2O_3 (d), ZrO_2 (e), MnO (f) and ZnO (g) with well developed crystal of Sr_3AH_6 (h).

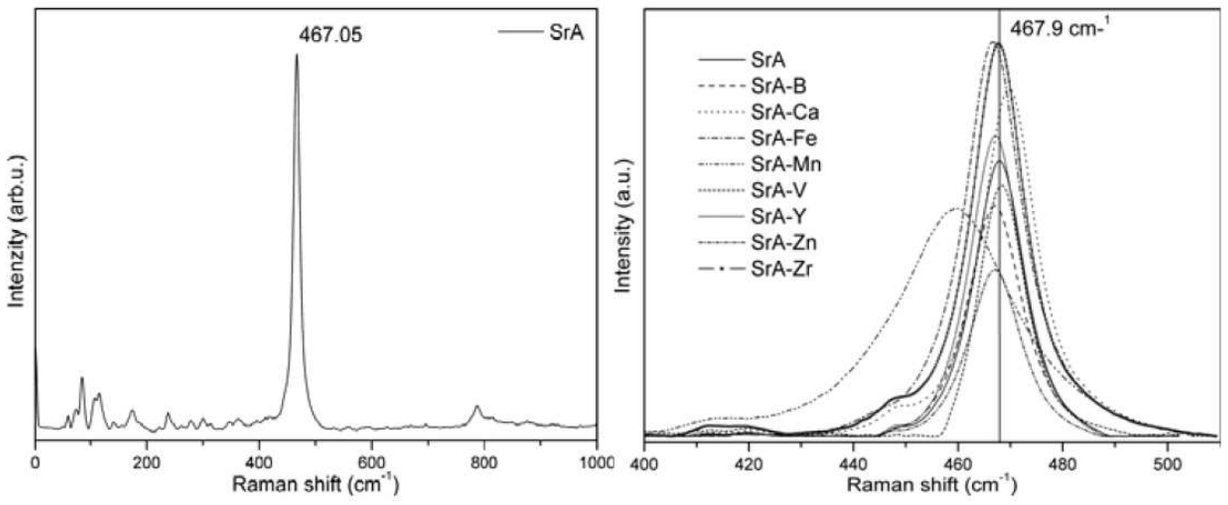

Figure 30. Raman spectra of $SrAl_2O_4$ phase (a) and doped Sr Al O_4 structures (b) (where=Ca, Zn, Mn and=B, Fe, V, Y, Zr in substitution of 5 wt.%).

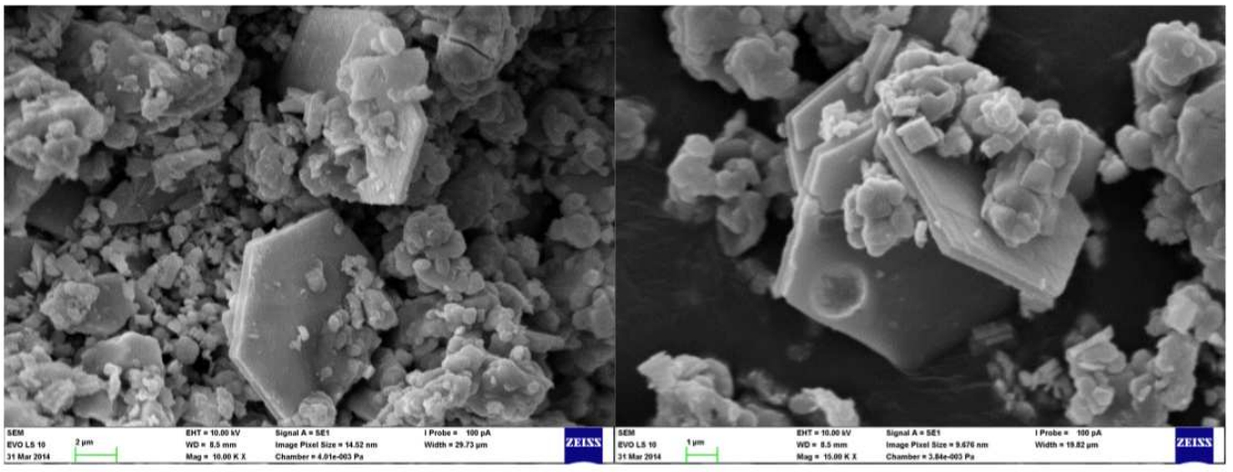

Figure 31. Large hexagonal plates of $Sr_2AH_x$of hydrated cement stone with 10 % of boron.

3.3. Substitution of SrO by CaO

The substitution of Sr^{2+}in the structure of strontium aluminate by Ca^{2+} (1, 5 and 10 %) introduced as $CaCO_3$ into the raw meal leads to the substitutions in the Sr_3A during thermal processing of clinker. The content of calcium in formed solid solution of $(Sr_{3-x}Ca_x)A$ (where=0.34 (1%), 1.02 (5%) and 1.12 (10%)) increases with the extent of substitution, whereas the content of the $(Sr_{3-x}Ca_x)A$ phase decreases (Fig.32(a)). In other words, the introduction of $CaCO_3$ into the raw meal suppresses the formation of tristrontium aluminate phase during the thermal processing of clinker.

The main diffraction lines of strontium aluminate (-211, 220 and 211) are shifted to the higher position on the °2Θ scale with increasing amount of Sr^{2+}cations substituted by Ca^{2+} (Fig. 32(b)). Therefore the introduction of smaller ions (Table 1 in Chapter 8) of higher electrone-

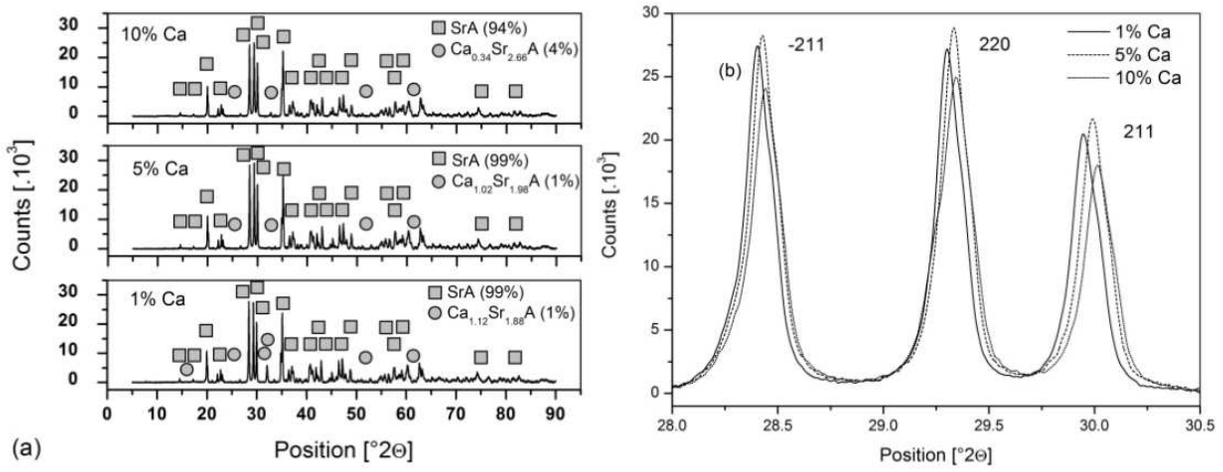

Figure 32. XRD analysis of strontium aluminate clinker doped by calcium.

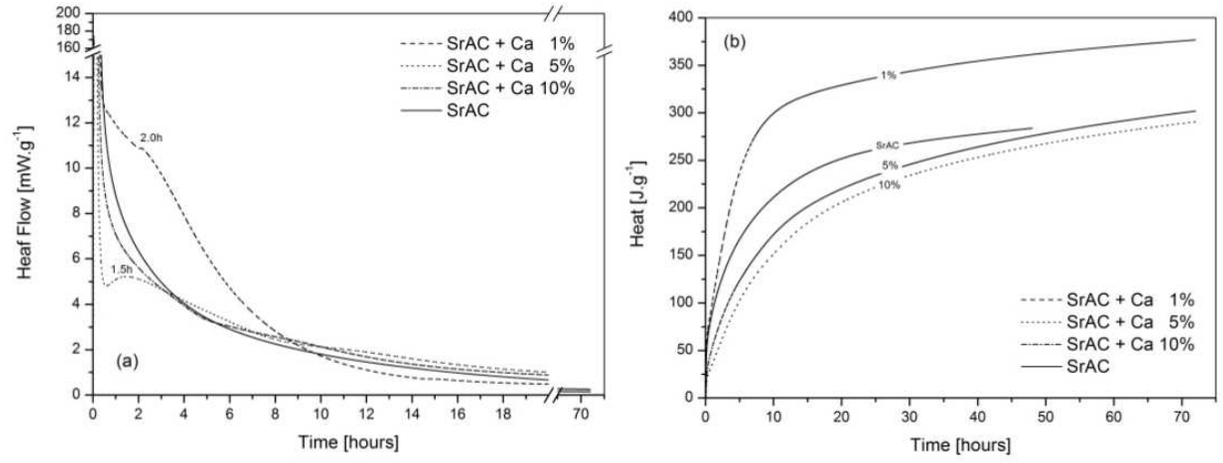

Figure 33. Heat flow (a) and heat of hydration (b) for the samples doped with calcium.

gativity leads to the decrease of volume of basic cell unit of strontium aluminate. That leads to lower reactivity with water (Fig.33, please refer to the discussion in Chapter 5.6 related to the size of opened channels in the structure of SrA and their influence on the reactivity with water).

The hydration of prepared samples was investigated by isothermal calorimetry at the temperature of 25°C for the first 72 h of hydration (Fig.33). The decrease of hydration heat (b) for the sample prepared with 5 and 10 % of calcium can be observed as the consequence of higher thermodynamic stability (please see the discussion in Chapter 1.2.4) as well as decreasing amount of formed $(Sr_{3-x}Ca_x)A$ solid solution.

The course of hydration of the sample prepared with 1% of calcium supports the results of X-ray diffraction analysis (Fig.32) indicating that the substitution in the Sr_3A structure proceeds prior to the substitution in the structure of SrA. That can be also explained via the mechanism of formation of SrA phase (please reffer to Fig.24 and the corresponding discus-

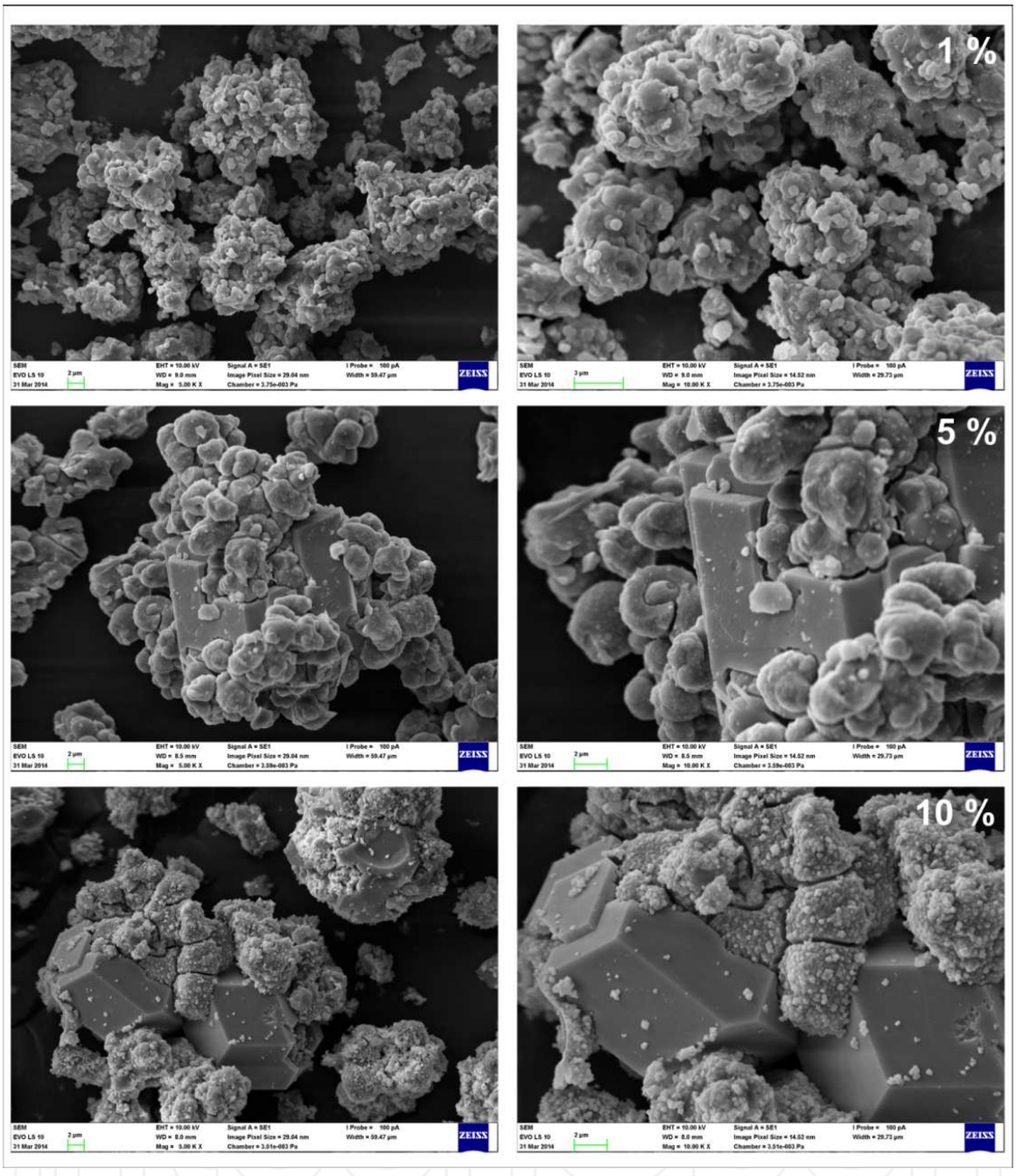

Figure 34. Electron microscopy of hydrated cement stone of clinker prepared with 1, 5 and 10% of Sr^{2+}substituted by Ca^{2+}.

sion in Chapter 4). The highest content of formed solid solution of $(Sr_{2.66}Ca_{0.34})A$[4] (Fig.32a) which has lower reactivity with water than SrA provides the explanation for the heat flow released from the sample upon hydration (please compare the heat released from SrA and Sr_3A, Fig.12 in Chapter 5).

4 Calcium has approximately two-fold dissolution heat than strontium.

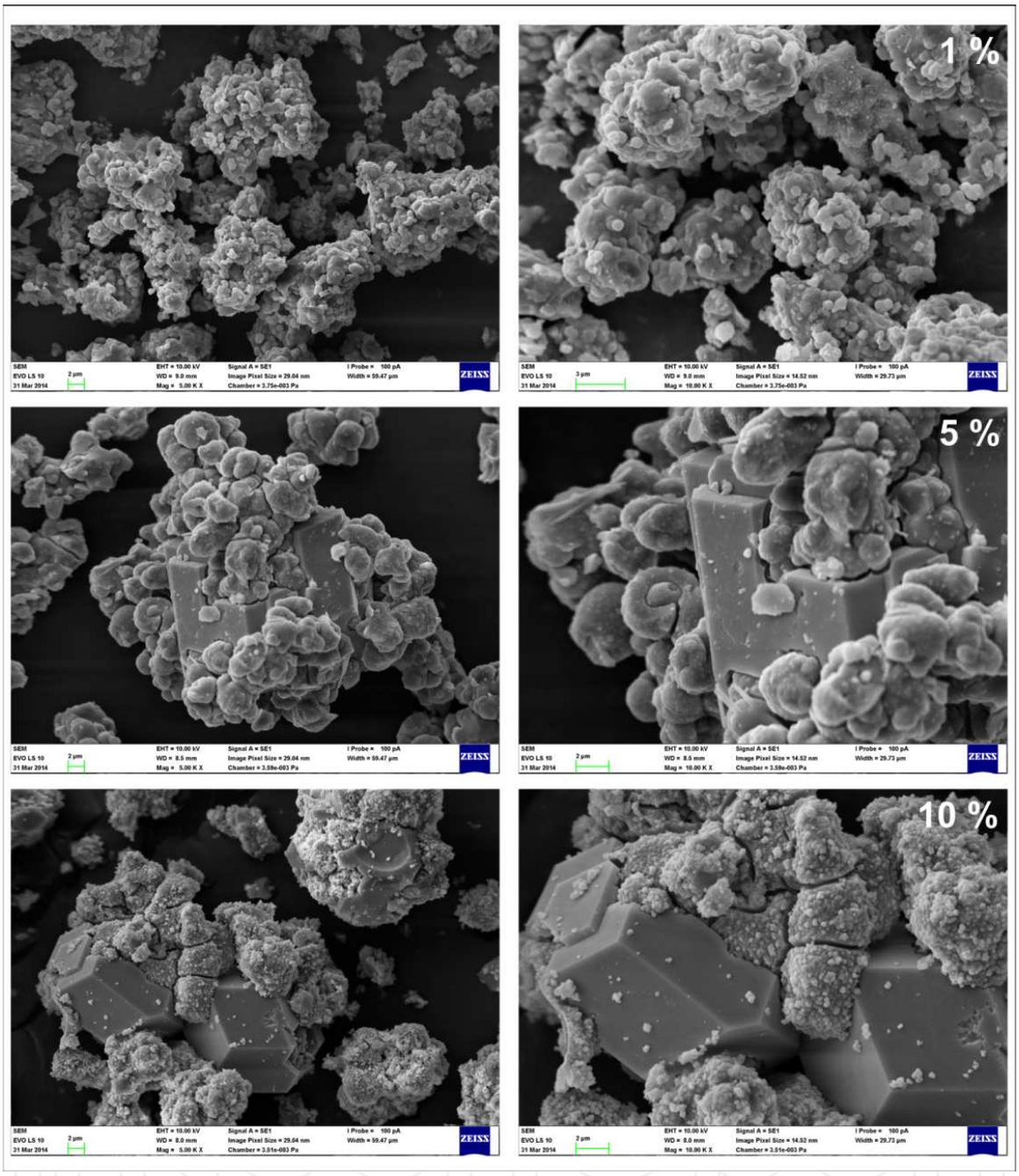

Figure 35. WDX analysis of hydrogarnet crystal formed during the hydration of strontium aluminate clinker prepared with 10 % of Ca^{2+}.

The maximum of main hydration effect, which appearsat 1.5 h for the sample prepared with 10% of calcium indicates, that the hydration properties are more similar to those of CAC as the content of Ca^{2+}ions in formed solid solution increases.

The hydrogarnet phase $(Sr_{3-x}Ca_x)AH_6$ and AH_3 are recognized as the main products of hydration of prepared clinker. Electron microscopy (Fig.34) shows the formation of well developed crystals of hydrogarnet phase in the samples prepared with 5 and 10% of Sr^{2+}

substituted by Ca^{2+}. Combining these results with previously described influence of Ca^{2+} ions on the formation of Sr_3A phase, the crucial role of lack of tristrontium aluminate and lower reactivity of Ca-substituted SrA in the nucleation and growth of large hydrogarnet crystals at the beginning of hydration process can be supposed.

Fig.35shows the composition of hydration product of strontium aluminate clinker prepared with 10% of Ca^{2+}. The (Sr+Ca):Al atomic ratio ~3:2 corresponds to the formation of Ca-substituted tristrontium aluminate hexahydrate with the composition given by the formula $(Sr_{2.7}Ca_{0.3})AH_6$. Therefore, Ca^{2+} ions substitute Sr^{2+} in the hydrogarnet phase in the ratio corresponding to the amount of cations substituted in the original clinker (10 %).

IntechOpen